

Cite this: *J. Mater. Chem. A*, 2023, **11**, 6772

## Recent development and emerging applications of robust biomimetic superhydrophobic wood

Xiaojun Li,<sup>a</sup> Likun Gao,<sup>a</sup> Min Wang,<sup>a</sup> Dong Lv,<sup>a</sup> Peiyao He,<sup>a</sup> Yanjun Xie,<sup>a</sup> Xianxu Zhan,<sup>\*c</sup> Jian Li<sup>a</sup> and Zhiqun Lin<sup>\*b</sup>

The properties of superhydrophobic wood depend heavily on the design of micro roughness and low-surface-energy chemical components via various fabrication strategies. However, the commercial development of these materials is still restricted by imprecise durability results due to the inadequate standard system. Some appealing applications, where water repellency is required, have been explored to extend the functionality of superhydrophobic wood. In this review, the recent progress in preparing superhydrophobic wood, including graft copolymerization, chemical vapor deposition, hydrothermal synthesis, sol-gel methods, template methods, dip coating, and spraying methods, is summarized, emphasizing the comprehensive understanding of the superhydrophobic mechanisms based on roughness and surface energy. The widely applied tests to evaluate the mechanical and chemical durability of superhydrophobic coatings such as sand abrasion resistance tests, tape peel tests, pencil hardness tests, corrosion resistance tests, and UV resistance tests, are introduced. The development of superhydrophobic wood facilitates its emerging applications in anti-icing, oil-water separation, self-healing, and energy storage and conversion. As such, this review provides fundamental guidelines for designing superhydrophobic wood.

Received 18th December 2022  
Accepted 24th February 2023

DOI: 10.1039/d2ta09828h

rsc.li/materials-a

### 1. Introduction

During the long evolutionary process, organisms have undergone the evolution of their functional structures and surface states, which is inevitable for adapting to the changing environment. For example, many surfaces of plants and animals exhibit superhydrophobic properties, such as lotus leaves, mussels, butterfly wings, water strider legs, and nepenthes.<sup>1-5</sup> These superhydrophobic phenomena have thoroughly proven that the micron-sized papillary structures on the surface and waxy hydrophobic substances of surfaces such as the lotus leaf would cause the water droplets to fall off the lotus leaf, accompanied by carrying away dust or other substances and resulting in a self-cleaning effect. Based on the extensive exploration and analysis of this specific functional phenomenon from nature, German scientists, Barthlott *et al.* first proposed the “lotus effect” in 1997, which was then considered a special wetting property.<sup>6</sup> The biomimetic superhydrophobic surfaces with water contact angle larger than 150° are artificially manufactured to possess micro-/nanoscale hierarchical structures and low surface energy, representing promising materials

for a wide range of applications including high-altitude self-cleaning glass, anti-icing superhydrophobic coating for outdoor wooden fences, anti-corrosion materials for ships and crude oil pipeline transportation, *etc.*<sup>7-10</sup>

With further studies on superhydrophobic coatings, the multi-functional coatings achieved via numerous methods have become more pronounced in various fields. For example, Zhang *et al.* found that the as-prepared superhydrophobic coating possessing UV aging stability and anti-icing abilities through the phase separation method could delay ice formation and weaken the ice adhesion. Such superhydrophobic coatings have been proposed to protect the 1000 kV high-voltage transmission towers.<sup>11,12</sup> The superhydrophobic coatings prepared with attapulgite nanorods, polypyrrole, hexadecyl polysiloxane and silicone resin also exhibited superior anti-icing performances due to the synergy of photothermal ability, superhydrophobicity and durability, which are promising in various practical applications.<sup>13</sup> Similarly, they designed the anti-corrosion superhydrophobic coatings using modified epoxy resin paint, which are promising for metal protection.<sup>14,15</sup> Superhydrophobic coatings have also been explored for the superLE(liquid electrolyte)philic/superhydrophobic and thermostable separators,<sup>16</sup> oil pipelines, power lines and airplane wings,<sup>17</sup> self-cleaning solar cells,<sup>18</sup> solar nano-coatings for eliminating ice on the cables,<sup>19</sup> *etc.* However, although multifunctional superhydrophobic coatings are expected in many applications, it should be noted that different components would induce

<sup>a</sup>Key Laboratory of Bio-based Material Science & Technology, Ministry of Education, Northeast Forestry University, Harbin 150040, PR China. E-mail: gaolk@nefu.edu.cn

<sup>b</sup>Department of Chemical and Biomolecular Engineering, National University of Singapore, Singapore 117585, Singapore. E-mail: z.lin@nus.edu.sg

<sup>c</sup>Dehua TB New Decoration Material Co., Ltd, Huzhou 313200, PR China



interface competition in binding. Exploring the interfacial properties of materials and precisely controlling the temperature and duration of the spraying and curing of multi-layer coatings are critical in the development of multifunctional superhydrophobic coatings.

Durability issues have restricted the applications of superhydrophobic coatings and have attracted lots of attention.<sup>20–23</sup> The mechanical strength of substrates and the attachment forces between the coatings and the substrates are the keys to designing durable superhydrophobic surfaces. Specific descriptions of durable resistance and exact durability test parameters are still lacking. Although several international standards are focused on the abrasion resistance of furniture spray paint, the precise characterization methods should be proposed for different superhydrophobic materials surfaces that are prepared with various microstructures and chemicals. Judging the range of mechanical strengths that the substrates can withstand may be useful for guiding the durability tests of various superhydrophobic surfaces.<sup>20</sup> Besides, the superhydrophobic coatings with self-healing properties can regenerate the superhydrophobicity after being subjected to mechanical wear, thus improving mechanical durability.<sup>21</sup> Recently, some studies have reported that the micro-skeleton-nanofiller film with high-strength 3D porous structure can provide excellent durable mechanical properties.<sup>24</sup> The high mechanical strength originates from the strong covalent bonding between the superhydrophobic medium and the porous skeleton.

As a renewable and environmentally-friendly material that is extensively applied in interior and exterior decoration and construction, superhydrophobic wood exhibits superior liquid-repellant properties and extended service life in practical applications, which improve the intrinsic defects of wood, such as the deformation caused by hydrophilicity, and the cracking and warping caused by water loss and susceptibility to mold.<sup>25–27</sup> However, wood-based superhydrophobic coatings tend to show mechanical and chemical frailty. Under mechanical load or chemical attack, the superhydrophobicity of contact areas is greatly reduced, thereby destroying the superhydrophobic surface and limiting their practical applications. Therefore, the mechanical robustness and chemical durability of superhydrophobic wood surfaces are crucial for practical applications. In addition, for some special applications, wood-based superhydrophobic coatings require not only high transparency, environmental friendliness, and non-toxicity, but also multifunctionality, such as anti-icing properties used in a winter snow environment, and self-healing properties used under frequent working conditions. Recently, it has been reported that the designed wood surfaces possessing photothermal effects could enhance the durability and also endow the materials with anti-icing, oil–water separation/crude oil recovery, self-healing, and UV shielding properties.<sup>28–32</sup> The recent progress of superhydrophobic surfaces has greatly promoted the emerging applications of wood products, especially in energy storage and conversion fields, such as electrocatalysis and nanogenerators.

In this review, we introduce a variety of preparation methods, durability tests, and the emerging applications of



Fig. 1 Schematic illustration of the development and emerging applications of biomimetic superhydrophobic wood, including a variety of preparation strategies, durability tests, and representative emerging applications.

superhydrophobic wood with additional photothermal effects or energy storage and conversion (summarized in Fig. 1), aiming to establish guidelines for the comprehensive understanding and practical applications of superhydrophobic wood. The challenges and opportunities to potentially advance the rational design of durable and multifunctional superhydrophobic wood are also discussed.

## 2. Synthesis strategies

According to the reported superhydrophobic mechanism, enhancing the durability of superhydrophobic surfaces is the most effective way to maintain superhydrophobicity by keeping the micro–nano hierarchical structure intact and reducing the surface energy.<sup>33–35</sup> There are diverse methods with their own advantages for constructing rough surfaces with microstructures and low chemical energy. Covalent bonds can be generated between the substrates and coatings through the graft copolymerization method, while the film-forming rate could be increased and the chemical reagents could be reduced through chemical vapor deposition. If nanomaterials are required, the hydrothermal synthesis methods would be more suitable. The stability of superhydrophobic solutions and the compatibility between the substrates and the hydrophobic agents could be well modulated *via* the sol–gel method. Recently, there have been many reports that the roughness of a surface could be greatly increased through templating/etching methods. Notably, the exploration of spraying and dip-coating methods provides possibilities for industrially preparing superhydrophobic coatings. In this section, we present the advances in methods such as graft copolymerization, wet chemical



methods (chemical vapor deposition, hydrothermal synthesis, and sol-gel), the template method and surface coating method (dip coating and spraying), for the design and fabrication of durable superhydrophobic surfaces.

## 2.1 Graft copolymerization method

Graft copolymerization is a chemical reaction in which long chains of different polymer species are combined in covalent bonds. It is known that there is a large number of hydroxyl and carboxyl reactive groups on the surfaces of wood's main components (cellulose, hemicellulose, and lignin). This is beneficial for the superhydrophobic coatings to be firmly grafted onto the wood through covalent bonds, which are formed by chemical reactions between the above-mentioned reactive groups of wood and the low surface energy substances.

Based on graft copolymerization, researchers have made progress in the fabrication of robust superhydrophobic wood. For example, Wang *et al.* grafted long-chain octadecyl isocyanate (OTI) onto wood cell walls accompanied by the formation of polyurethane bonds (Fig. 2a), which could reduce the surface energy and improve the dimensional stability of wood, resulting in enhanced chemical resistance, stability, physical and chemical durability.<sup>36</sup> Wang *et al.* found that the atom transfer radical polymerization (ATRP) reaction could be an effective strategy for the grafting of the low-surface-energy agent, poly(2-(perfluorooctyl)ethyl methacrylate) (PFOEMA), onto wood through (Fig. 2b).<sup>37</sup> The as-prepared superhydrophobic wood presented an extended service life of 15 days after various durability tests, including mildew-resistance tests, finger wiping, and the tests

of tape adhesion, knife scraping and sandpaper abrasion. Additionally, the products showed great potential in the applications of self-cleaning. In another study, Wang *et al.* used a silicon oxide ( $\text{SiO}_2$ ) layer to modify the original wood surface and the hydrolyzed  $\text{SiO}_2$  provided more hydroxyl groups ( $\text{Si-OH}$ ), leading to enriched surficial hydroxyl groups of the wood.<sup>38</sup> Polydimethylsiloxane (PDMS) was fabricated by the acid-catalyzed polymerization of dimethyldimethoxysilane (DMDEOS), then grafted onto the modified surface by covalent bonds, which were produced as the  $\text{Si-O}$  groups in PDMS came in contact and reacted with the  $\text{Si-OH}$  in the  $\text{SiO}_2$  layer (Fig. 2c). After the above modification processes, the wood surface achieved superior superhydrophobic performances. Due to the rearrangement of PDMS chains after plasma treatment, the superhydrophobic coatings combined with PDMS and  $\text{SiO}_2$  layer exhibited self-healing properties that could further protect the wood substrates. Specifically, Meng *et al.* fabricated lignin-based petaloid nanoflakes (LPNFs) with superhydrophobic effects by polymerizing the crystallized lignin stearyl esters (LSEs).<sup>39</sup> In this case, the original lignin was esterified with stearyl chloride in pyridine, and their volume ratio in the solvent was carefully controlled to modulate the stearyl grafting level in LSEs, which is prone to an organized self-assembling ability and remarkable hydrophobicity of LPNFs (Fig. 2d).

Recently, Wu *et al.* presented a novel method of fabricating self-healing superhydrophobic wood surfaces.<sup>40</sup> According to the study, the microcapsules (MC) constituted of low-surface-energy polytetrafluoroethylene (PTFE) coated by vinyltriethoxysilane (VTES) were firstly produced through emulsion

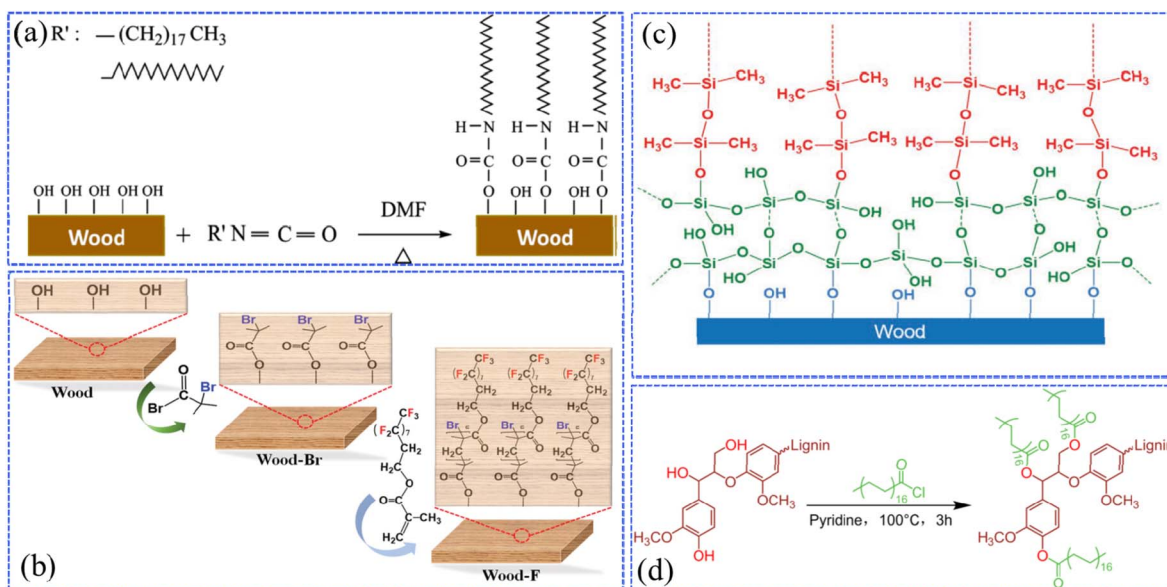


Fig. 2 (a) Schematic diagram of durable superhydrophobic wood, where OTI is grafted onto wood cell walls *via* polyurethane bonds. Reproduced with permission from ref. 36. Copyright 2017, Springer Verlag. (b) Illustration of the atom transfer radical polymerization (ATRP) reaction for preparing the superhydrophobic wood using poly(2-(perfluorooctyl)ethyl methacrylate) (PFOEMA) as a low-surface-energy agent. Reproduced with permission from ref. 37. Copyright 2020, Walter de Gruyter GmbH. (c) Schematic representation of the wood silanized by silicon oxide and then covalently bound to PDMS. Reproduced with permission from ref. 38. Copyright 2018, Wiley-VCH. (d) A graphical representation of the esterification reaction of the original lignin with stearyl chloride in pyridine. Reproduced with permission from ref. 39. Copyright 2022, Elsevier.





polymerization. Then, acetic acid and stearic acid were added to the homo-dispersed composite of MC, PTFE, and zinc oxide (ZnO) to achieve the hydrophobicity, of which the carboxyl group in acetic acid reacted with the free hydroxyl group of zinc oxide and thus the resulting  $\text{Zn}^+$  further reacted with the stearic acid, leading to the grafting of a micron-sized flower-like zinc stearate ( $\text{ZnSt}_2$ ) arrangement with  $-\text{CH}_3$  hydrophobic groups onto the surface of the wood. More interestingly, the wear resistance and the corrosion resistance test proved that the superhydrophobic coating was based on the wood possessing self-healing capabilities, which were mainly due to the restoration of the flower-like structure on the surface by the impregnation with stearic acid solution and the supplementation of low surface energy substances on the surface of the coating through the damage to the microcapsules. As the author described, such wood-based hydrophobic treatment technology can be used in wooden furniture, wooden structural buildings, and the preservation of historical sites. Wang *et al.* synthesized a hydrophobic agent, that is, a silica/wax emulsion ( $\text{PPW}@\text{SiO}_2$ ) composite, which consisted of polypropylene wax (PPW) grafted with maleic anhydride and nano-silica ( $\text{SiO}_2$ ).<sup>41</sup> Then, a deeply hydrophobic wood was achieved through the heat infiltration and thermal compression of the fast-growing poplar trees. Herein, PPW and  $\text{SiO}_2$  nanoparticles worked together to create a micro/nano multi-layered rough structure on the wood surface, resulting in improved hydrophobic properties. As reported by Wu *et al.*, the composite coatings consisting of waterborne ultraviolet lacquer product (WUV) as the main material, zinc oxide (ZnO) as the additive, and stearic acid as the surface modifier, were used to prepare a highly corrosion-resistant superhydrophobic poplar wood ( $\text{WUV}/\text{ZnSt}_2/\text{Wood}$ ).<sup>42</sup> The prepared superhydrophobic surface could retain superior superhydrophobicity even after 50 h immersion in an alkaline solution with  $\text{pH} = 9$ . Li *et al.* prepared the UV-resistant superhydrophobic wood by using the hydrophobic agent (polydimethylsiloxane, PDMS) and the cross-linked monomer ( $\gamma$ -methacryloxypropyltrimethoxysilane, MAPS).<sup>43</sup> These two materials could promote the linkage between the  $\text{TiO}_2$  particle layer and wood substrate due to the covalent bond generated after electron beam irradiation.

## 2.2 Wet chemical method

The wet chemical method, including chemical vapor deposition (CVD), hydrothermal synthesis, the sol-gel process, *etc.*, is widely applied to fabricate various superhydrophobic surfaces. In the following sections, we outline the recent findings pertaining to superhydrophobic wood fabricated through wet chemical methods.

**2.2.1 Chemical vapor deposition.** Chemical vapor deposition (CVD) is a facile method for the surfaces of substrates covered by superhydrophobic films, in which the superhydrophobic films are formed by the reaction of two or more chemicals in the form of gas or vapor.<sup>44</sup> In this case, the final superhydrophobic degree can be controlled by adjusting the composition of the gaseous chemical materials.<sup>45</sup> The CVD technology is beneficial for the patterned or rough surfaces of

the desired material, which are better covered by thin superhydrophobic films with relatively low chemical consumption.<sup>46</sup> In the case of wood substrates modified by CVD, a micro/nanoscale rough film could be constructed on the surface, while the chemical reactions of fluorination, silylation, *etc.*, would easily occur to reduce its surface free energy.<sup>47–49</sup> However, although this technology could reach high film formation rates, a certain amount of heat resistance of the substrates and high equipment costs are required, thus limiting the practical applications.

Zhang *et al.* prepared a luminescent and superhydrophobic bifunctional coating material with the modified  $\text{SrAl}_2\text{O}_4:\text{Eu}^{2+}$ ,  $\text{Dy}^{3+}$  (SAOED) phosphor.<sup>47</sup> As functional filters, SAOED phosphors with excellent afterglow luminescence properties were hydrophobically treated through a silica modification method based on tetraethyl orthosilicate (TEOS) and (3-aminopropyl) trimethoxysilane (APTMS). A facile two-step combination of spraying and vapor deposition was adopted to settle the above nanoscale rough superhydrophobic coatings onto wood surfaces (Fig. 3a). It is worth noting that such luminescent superhydrophobic wood-based products are suitable for practical applications in interior decoration, smart ceilings, and luminescence labeling. For ultrathin and easily broken materials, CVD could be a non-destructive technology for constructing superhydrophobicity. As reported by Zhou *et al.*, a rapid and simple surface modification of paper was conducted without organic solvents by forming a small amount of hydrophobic modifying reagent (heptadecafluoro-1,1,2,2-decyl) triethoxysilane (HFTTES) in vapor in a confined space during the CVD process.<sup>50</sup> The gaseous hydrophobic reagent reacted with the active hydroxyl groups on a paper surface, resulting in the successful deposition of silicon tetrachloride that shows low surface energy. The water-resistance property could be modulated by controlling the CVD deposition time and thus changing the surface roughness. Wang *et al.* prepared simple wood-based superhydrophobic coatings with rough structures by depositing ZnO on the wood surface and then modifying the surface ZnO with stearic acid.<sup>51</sup>

To enhance the high-temperature resistance, the modification of the surface coating with inorganic materials, such as nanofibrillated cellulose (NFC), carbon nanotubes (CNTs), and other novel materials, has attracted significant attention. For example, Huang *et al.* successively pre-sprayed a commercial spray paint used as an adhesive and nanofibrillated cellulose (NFC) ethanol suspension onto a poplar plywood surface and then deposited the modification agent (1H,1H,2H,2H-perfluoroethyltrichlorosilane) with the ability to reduce the surface energy through the CVD method (Fig. 3b).<sup>48</sup> In detail, during the drying of the NFC ethanol suspension, the alcohol in the suspension volatilized and the spray paint cured with the increasing temperature, and then a rough layer firmly covered the wood surface. After the above operation, the obtained superhydrophobic wood presented excellent mechanical properties, UV radiation resistance and high-temperature resistance as 1H,1H,2H,2H-perfluoroethyltrichlorosilane overcame the problems of the poor wear resistance and durability of NFC. Zhu *et al.* developed a novel superhydrophobic wood aerogel with



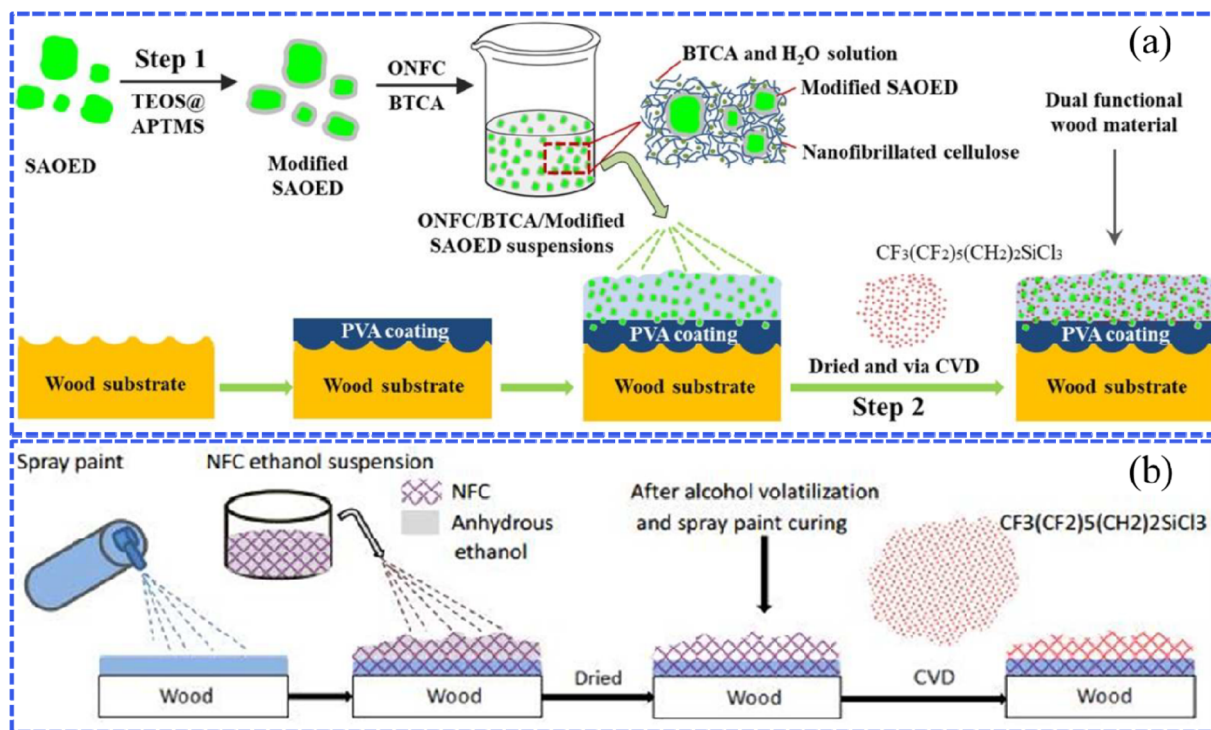


Fig. 3 (a) Schematic diagram showing the preparation of bifunctional wood that possesses superhydrophobic and fluorescence properties, which was treated with the modified  $\text{SrAl}_2\text{O}_4 \cdot \text{Eu}^{2+} \text{Dy}^{3+}$  SAOED phosphor. Reproduced with permission from ref. 47. Copyright 2018, Elsevier. (b) A sketch of the preparation procedure for superhydrophobic nanofibrillated cellulose (NFC) coatings *via* the chemical vapor deposition (CVD) method. Reproduced with permission from ref. 48. Copyright 2016, Royal Society of Chemistry.

thermal management performance by the chemical vapor deposition of ethyltrimethoxysilane (MTMS) and subsequent splicing with PDMS-modified carbon nanotubes (CNTs).<sup>52</sup> The combination of the lipophilic nature of the wood aerogel and CNT with the intrinsic photothermal effect provided an optimum combination of adsorption, rapid volatilization, and accelerated purification, which was key to continuously removing oil from the aerogel in gaseous form and preventing the aerogel from reaching its saturation point of oil absorption.

**2.2.2 Hydrothermal synthesis.** As a relatively mature and simple synthesis technology, hydrothermal synthesis has been extensively studied for creating crystalline particles with microscale or nanoscale roughness on the substrate surfaces at high temperatures. The ideal rough micro/nanostructure can be obtained by controlling the reaction time and temperature during the synthesis process. However, attention should be paid to the “surface competition” between the materials.

For example, Gao *et al.* constructed a robust superhydrophobic wood by combining the low-temperature hydrothermal synthesis of  $\text{TiO}_2$  particles to improve the surface roughness and the modification using (heptadecafluoro-1,1,2,2-tetradecyl)trimethoxysilane (FAS) to reduce the surface energy (Fig. 4a).<sup>53</sup> As reported by the researchers, the further binary combination of Ag nanoparticles through the silver mirror reaction could obtain much rougher Ag- $\text{TiO}_2$  heterostructures on the surface of wood substrates.<sup>54,55</sup> In the durability test, the superhydrophobic wood could maintain stability in acids (pH = 1) and at high temperatures (150 °C). Similarly, Lu *et al.*

conducted the hydrothermal *in situ* synthesis of  $\text{Cu}_2(\text{OH})_3\text{Cl}$  nanoparticles based on the surface of camphor wood and then impregnated them in the ethanolic solution of stearic acid/epoxy resin (STA/EP) to achieve superhydrophobic effects (Fig. 4b).<sup>56</sup> Sun *et al.* presented the *in situ* synthesis of  $\text{WO}_3$  nanostructures on wood surfaces by a two-step hydrothermal process at different temperatures (90 °C and 120 °C) for 6 hours; they achieved a novel wood material with  $\text{WO}_3$  content of 12.89 wt% ( $\text{WO}_3$ -coated wood) possessing both superhydrophobic properties and the photochromic effect.<sup>57</sup> Wang *et al.* synthesized  $\alpha\text{-FeOOH}$  films on the wood surface *via* the hydrothermal reaction of iron sulfate and urea and settled self-assembled octadecyltrichlorosilane (OTS) monolayers on the as-prepared surface.<sup>58</sup> The as-prepared superhydrophobic wood also exhibited excellent resistance to acid and alkali corrosion. Liu *et al.* utilized wood as the substrate and covered it with  $\text{TiO}_2$  film through a one-step hydrothermal process.<sup>59</sup> Note that the porous structure of wood is the key to obtaining superhydrophobic performance by the synthesis technology, that is to say, it is also suitable for other porous materials, such as fibers, papers, *etc.*

**2.2.3 Sol-gel method.** The sol-gel method is a reaction based on the use of highly chemically active compounds as precursors for the formation of the gel with a three-dimensional network-like structure. Firstly, the various liquid precursors are hydrolyzed, condensed, or undergo other chemical reactions, and then a stable, transparent sol system in solution is produced. Finally, a slow polymerization between the aged



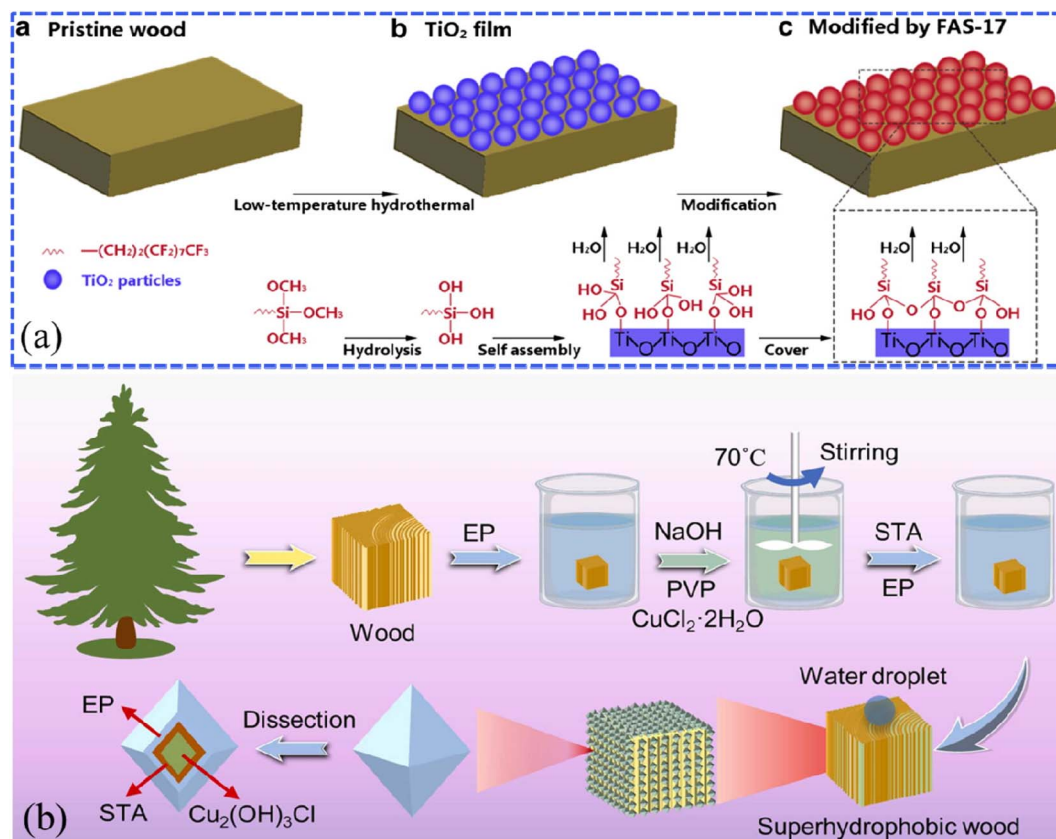


Fig. 4 (a) Schematic illustration of the fabrication of superhydrophobic wood using  $\text{TiO}_2$  and (heptadecafluoro-1,1,2,2-tetradecyl)trimethoxysilane (FAS-17). Reproduced with permission from ref. 53. Copyright 2014, Elsevier. (b) A schematic diagram of the *in situ* hydrothermal synthesis of  $\text{Cu}_2(\text{OH})_3\text{Cl}$  nanoparticles onto a pine wood surface. Reproduced with permission from ref. 56. Copyright 2022, Elsevier.

precursor particles occurs over time to form a gel with a three-dimensional network-like structure. After curing *via* drying or other means, the material with a nano-level structure can be prepared.

In recent years, the sol-gel technology has attracted a lot of attention for fabricating durable superhydrophobic wood for the above reasons. For example, Li *et al.* presented a robust superhydrophobic wood surface with a multi-level micro/nano-roughness structure by *in situ* mineralization and polymerization using a simple sol-gel method as well as an efficient electron beam (EB) curing technique.<sup>43</sup> According to the study, inorganic  $\text{TiO}_2$  particles were *in situ* deposited onto the wood substrate *via* sol-gel technology. The hydrophobic agent consisted of polydimethylsiloxane (PDMS) and the cross-linked monomer ( $\gamma$ -methacryloxypropyltrimethoxy silane, MAPS) was introduced by radiation crosslinking curing accompanied by creating new covalent bonds on the wood surface. On this basis, the wood could gain not only remarkable superhydrophobic performance but also significant ultraviolet (UV) resistance due to the  $\text{TiO}_2$  particles. Furthermore, the superhydrophobicity could endure harsh external conditions, such as abrasion tests under an 800 mesh sandpaper with a 200 g weight and moving 80 cm, and ultrasonication for more than 40 min, without destroying the multiscale micro/nanostructure, further proving the excellent wear resistance and robust mechanical durability of the superhydrophobic wood surface. Chang *et al.* applied

tetraethyl orthosilicate (TEOS) as an inorganic precursor and hexadecyltrimethoxysilane (HDTMS) as an organic modifier to prepare non-homogeneous nanocomposite coatings based on the wood surface by sol-gel chemistry.<sup>60</sup> Herein, the long-chain HDTMS not only acted as a hydrophobic agent to reduce the surface free energy of silica particles but also as a binder to aggregate nanoparticles through polymerization. The degree of aggregation of silica particles in the coating can be controlled by adjusting the initial concentration of HDTMS, thus modulating the surface morphology and roughness of the as-prepared superhydrophobic wood. Similarly, Wang *et al.* adopted a combination of the sol-gel method and vacuum-heating-cycles hydrothermal synthesis to deposit dense ZnO nanolayers on the spruce wood surface, thus obtaining superhydrophobic wood.<sup>61</sup> Wei *et al.* precisely synthesized  $\text{SiO}_2$  nanoparticles with an average diameter of  $\sim 110$  nm on a wood surface *via* a sol-gel process, then successively modified the wood with polydimethylsiloxane (PDMS) and (heptadecafluoro-1,1,2,2-tetradecyl) trimethoxysilane (17F) to achieve the superhydrophobic effect.<sup>62</sup>

### 2.3 Templating/etching method

The templating and etching methods are wet chemical reactions that involve the reactions of the liquid phase (solution) and solid phase (thin film). Using the templating method to





prepare a superhydrophobic wood surface requires constructing a layer with a rough structure that replicates the rough surfaces of templates, such as the papilla structure of the lotus leaf, the surface morphology of natural plants, *etc.*, then fixing the layers onto wood through repeating the operations of inversion, curing and peeling.<sup>63</sup> Gao *et al.* prepared lotus leaf-like superhydrophobic coatings on xylan-modified bamboo surfaces by using fresh lotus leaves and polydimethylsiloxane (PDMS) as templates and sealing *via* soft lithography.<sup>64</sup> As a result, the dimensional stability and superhydrophobic properties of the modified bamboo were significantly improved.

Inspired by the hierarchical and porous microstructure, wood has been directly used as structure templates to improve the roughness of the superhydrophobic coatings. For example, Wang *et al.* presented a facile and low-cost strategy to precisely produce structured PDMS superhydrophobic surfaces using microfine cross-sections of beech wood as a template (Fig. 5a) and controlled the degree of PDMS penetration within the wood capillaries by adjusting the PDMS pre-curing time to induce the formation of surface roughness at different pillar heights to achieve superhydrophobic effects.<sup>65</sup> The wettability of the PDMS surfaces was controlled by adjusting the PDMS pre-curing time of PDMS penetration within the wood capillaries, that is, the PDMS pillar heights. The results illustrated that the optimal pillar height of 229  $\mu\text{m}$  was confirmed to achieve the best hydrophobicity with the water contact angle reaching 156°. Apart from the above study, different wood microstructures such as willow wood, lauan wood and so on, treated through the calcination process, have also been applied as templates to prepare superhydrophobic coatings.<sup>66,67</sup> As reported by Wang *et al.*, pine and mango wood were calcined under inert gas conditions to obtain a carbon template with the remaining

porous wood structure.<sup>68</sup> A thick layer of copper was then electroplated onto the surface of the porous carbon template. After peeling off the copper layer, a microstructure mirroring the natural wood structure was achieved. Finally, the copper surface exhibited excellent hydrophobicity through modification with fluorosilane.

The etching technique is similar to the templating method, but the template is not required here, which makes it more facile. When processing the etching, the reactants in the solution will diffuse and chemically react with the surfaces of the substrates. Due to the fast corrosion rate, poor anisotropy, and low cost, the etching technique is prone to fabricate durable superhydrophobic materials. However, as a special matrix material, unlike metals that can be etched at high temperatures and pressures, wood is often combined with other synthetic methods to imprint complex microscale and nanoscale structures on its surface and then requires the etching of long chain groups to reduce surface energy. For example, Nie *et al.* hydrothermally synthesized ALOOH nanoparticles (Fig. 5b) and uniformly ground them with lignocellulose to obtain ALOOH nanoparticle/lignocellulose composite (ALC) sheets *via* a hot pressing process (Fig. 5c).<sup>69</sup> Polydimethylsiloxane (PDMS) was applied as a stamp to replicate the fresh lotus leaf template by soft lithography and then dipping it on the ALC surface. After solidification at 70 °C for 4 h, the PDMS seal was peeled off and a superhydrophobic ALC surface with biomimetic papillae structure (ALCP) was achieved (Fig. 5d). According to the results, hydrogen bonding interactions between the ALOOH NPs and lignocellulose could increase the mechanical properties and the condensation of the material, resulting in enhanced flame retardant properties. Therefore, the study provided a protective strategy for lignocellulose-based composites.

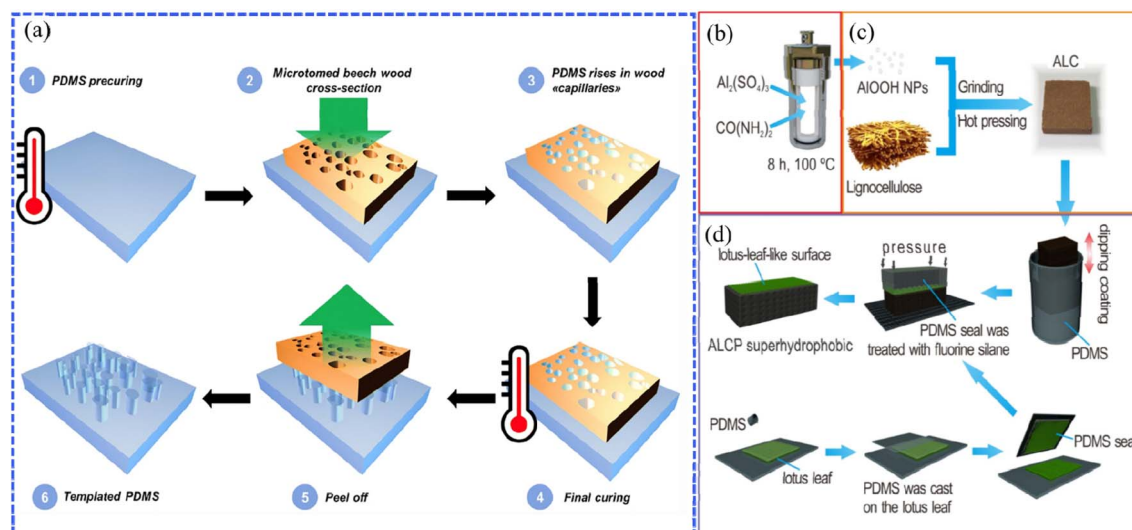


Fig. 5 (a) Illustration of the manufacture of PDMS material using beech wood as a template. Reproduced with permission from ref. 65. Copyright 2019, Springer Verlag. (b–d) Schematic illustration of the fabrication of ALOOH nanoparticle/lignocellulose composite (ALC) with a polydimethylsiloxane (PDMS) surface (ALCP) as a template, including (b) preparing ALOOH NPs through a hydrothermal reaction at 100 °C for 8 h, (c) grinding and hot pressing the mixture of ALOOH NPs and lignocellulose to fabricate ALC, and finally (d) fabricating ALCP through soft lithography based on the ALC surface. Reproduced with permission from ref. 69. Copyright 2019, Taylor and Francis Ltd.



## 2.4 Surface coating method

**2.4.1 Dip-coating method.** The dip-coating method is a facile method that involves immersing the substrate material into the prepared solution for a period of time and then taking it out to dry. The impregnation time could be reduced and the processing time decreased by heating, magnetic stirring, ultrasonic dispersion, and vacuum impregnation. For instance, Yao *et al.* first impregnated washed beech (WB) and washed pine (WP) into a cellulose stearyl ester (CSE) solution to endow them with hydrophobicity, that is, hydrophobic beech (HB) and hydrophobic pine (HP) were obtained.<sup>70</sup> After drying, a layer of glycerol stearyl ester (GSE) was brushed onto the wood to further create superhydrophobic HB (SHB) and superhydrophobic HP (SHP) (Fig. 6). The results illustrated that the wood that achieved superhydrophobicity could effectively resist fungal attack, while fungus could be found inside the untreated wood.

It has also been found that when the impregnated wood was placed into a superhydrophobic suspension containing

inorganic nanoparticles modified with low surface energy substances, the superhydrophobic coatings presented translucent and durable mechanical properties.<sup>71–74</sup> Arbatan *et al.* reported a two-step impregnation method for preparing superhydrophobic filter paper.<sup>75</sup> During the first step, an aqueous suspension containing precipitated calcium carbonate (PCC) pigments and cellulose nanofibers was used to impregnate the filter paper samples to form a very rough coated layer. Subsequently, the coated paper was treated with alkyl vinyl ketone dimer (AKD) in *n*-heptane solvent to complete the hydrophobic modification. Łukawski *et al.* achieved superhydrophobicity by dispersing carbon nanomaterials (carbon black (CB), graphene (Gr), and carbon nanotubes (CNTs)) in organic solvents (dichloromethane, DCM) by the dip-coating method, which allowed the formation of uniform carbon nanocoatings on any kind of wood.<sup>76</sup>

**2.4.2 Spraying.** The spraying method has been considered the simplest physical deposition method and is widely applied in industrial production. For practical wood processing, spraying is

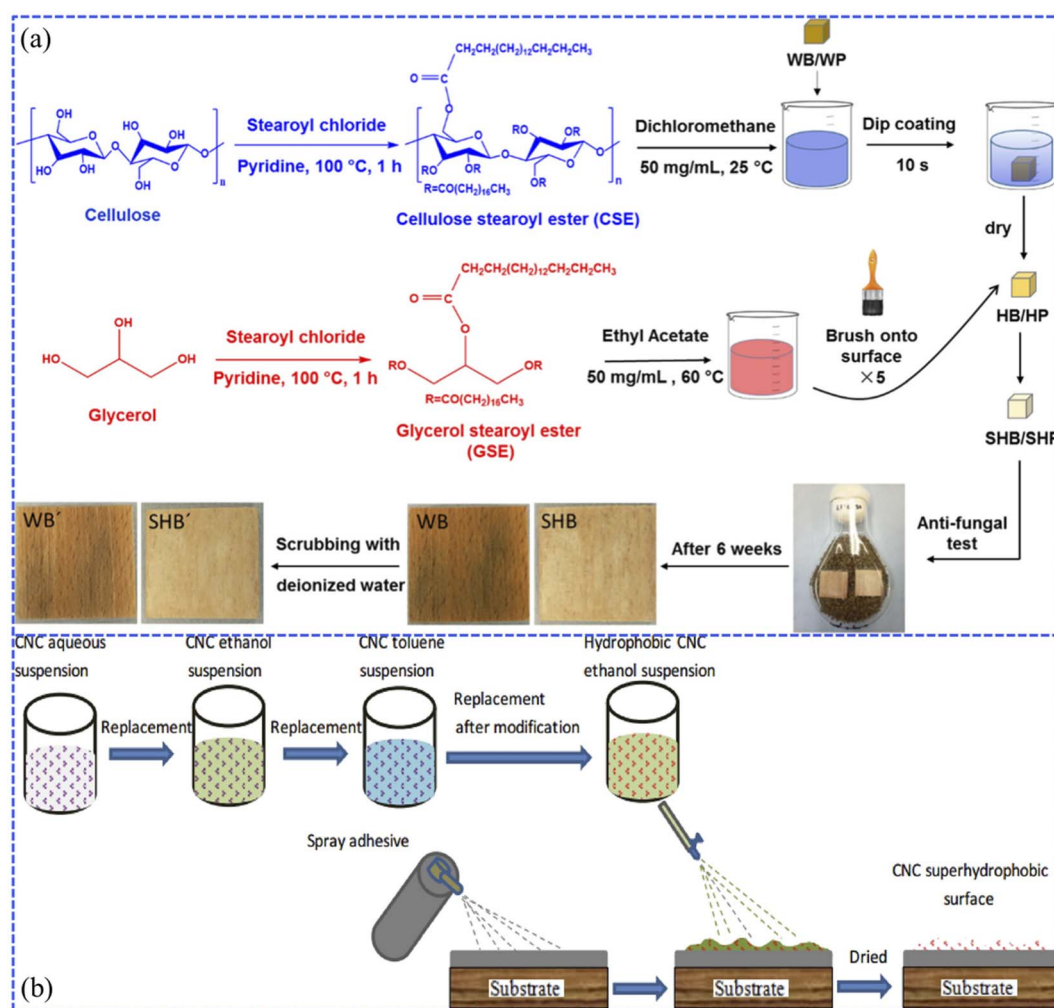


Fig. 6 (a) Synthesis schematic of hydrophobic and superhydrophobic wood (beech and pine) by dip-coating with cellulose stearyl ester (CSE) and glycerol stearyl ester (GSE). Reproduced with permission from ref. 70. Copyright 2019, Springer Netherlands. (b) Process diagram of the fabrication of the cellulose nanocrystal (CNC) superhydrophobic coating via spraying. Reproduced with permission from ref. 77. Copyright 2018, Elsevier.





Table 1 Summary of the synthesis parameters for spraying methods

| Substrates   | Spraying distance (cm) | Spraying pressure (kPa) | Particle size (nm) | Ref. |
|--|------------------------|-------------------------|--------------------|------|
| Cotton, cloths   | 15                     | 200                     | —                  | 87   |
| Metal, textile, wood   | 30 (vertical)          | 275                     | 5–50               | 101  |
| Wood   | 15                     | 200                     | —                  | 81   |
| Metal  | 10                     | 6000                    | 10–20              | 102  |
| Cotton fabric, paper, glass slide and other substrates                   | 12                     | 250                     | 15                 | 103  |
| Glass  | 10–20                  | 414                     | 15                 | 104  |
| Fabric, SSM, sponge, nickel foam, filter paper, ceramic, and wood        | 20                     | 138–207                 | 100                | 105  |
| Steel sheet, tile, wood and cotton fabrics                               | 10 (vertical)          | —                       | 15/25 (μm)         | 106  |
| Elastic substrate  | —                      | 27                      | 10                 | 107  |
| Glass slides   | 8–10                   | 200                     | —                  | 109  |
| Glass  | 15                     | 600                     | 20                 | 126  |
| Cloth  | 15                     | 300                     | 20                 | 127  |
| Wood ( <i>cunninghamia lanceolata</i> ), filter paper, fabric and cotton | Unlimited              | —                       | 25–300             | 128  |
| Al alloy plate   | ≤11 m                  | 48                      | 3–5 (μm)           | 129  |

one of the surface finishing methods for protecting the surfaces of wood-based products. Concerning superhydrophobic surfaces, a suspension of polymer and micron- or nano-sized particles is cast onto the surface of the substrate by spraying with a spray gun or airbrush. However, the thickness of the as-obtained superhydrophobic coating is generally thin and the roughness of the substrate surface is low, therefore mechanical durability is highly targeted to prolong the service life and minimize maintenance expenses. Recently, Huang *et al.* successfully created robust superhydrophobic coatings based on both wood and glass slides by a two-step spraying method.<sup>77</sup> In the study, the commercial spray paint (1*H*,1*H*,2*H*,2*H*-perfluorooctyltrichlorosilane, CF<sub>3</sub>-(CF<sub>2</sub>)<sub>5</sub>(CH<sub>2</sub>)<sub>2</sub>SiCl<sub>3</sub>) used as a binder was sprayed onto the substrates in advance (Fig. 6b), and the hydrophobically-modified cellulose nanocrystal (CNC) was then sprayed. The study not only provides the strategy for fabricating excellent superhydrophobic wood with self-cleaning properties and high mechanical strength but is also suitable for various materials, such as stainless steel mesh, which when coated with the binder and hydrophobic CNC was highly resistant to chemicals and UV radiation and could be applied in oil–water separation. Table 1 provides a representative summary of the recently reported parameters of the spray coating methods.

Additionally, the spray coating method can also be applied to prepare the superhydrophobic wood surface with a self-healing effect by spraying the healing agent, thus further protecting the wood from mechanical abrasion. For example, when the wood surface sprayed with perfluorooctyltriethoxysilane (KH1322)/silica composite suspension was subjected to mechanical wear, it could be restored to its self-healing ability by respraying a fluoroalkylsilane/silica composite suspension.<sup>78,79</sup>

More interestingly, some studies found that the cooperation between two and more preparation approaches could increase the thickness, adhesion and durability of the superhydrophobic coating to a greater extent, which may be due to the full combination between the wood surfaces and the chemical reagents during the fabrication processes. For example, Liu *et al.* prepared a robust superhydrophobic coating on a wood surface *via* the methods of spraying and thermal deposition.

The contact angle of the superhydrophobic wood was still larger than 150° even after several durability tests, such as the abrasion test, anti-corrosion and laundering test.<sup>81</sup> In addition, for better comparing the feasibility of various preparation approaches, a representative summary of the superhydrophobic performances including the water contact angles before and after different durability tests for the recently reported superhydrophobic coatings fabricated *via* the above-mentioned synthesis methods has been provided in Table 2. However, despite the proficiency in preparing the superhydrophobic coatings with contact angles higher than 150° and sliding angles less than 10° by optimizing the preparation methods, some undesirable durability results might be achieved through the homemade setups, thus causing the results to not be thoroughly comparable. This can be ascribed to the lack of uniform standard regulations, which requires further exploration.

### 3. Investigation of the durability of biomimetic superhydrophobic wood

It is well known that the function of man-made superhydrophobic materials will easily decrease when exposed to harsh mechanical or chemical conditions. The durability of superhydrophobic coatings has restricted the development of wood-based products due to their short application time and hence decreased potential costs. The mechanical and chemical durability tests have been investigated throughout the reported studies. The durable mechanism is acknowledged to be associated with the morphology of the superhydrophobic coatings and the chemical bonds between the hydrophobic composition and the substrate. Generally, these durabilities can be classified as mechanical durability including the ability to resist dynamic impact, and adherence to the substrates (sand abrasion resistance tests, tape peel tests and pencil hardness tests), as well as chemical durability including corrosion resistance, and UV resistance. Therefore, the categories of durability tests will be briefly discussed in detail below and are summarized in Tables



Table 2 Summary of the WCA and WSA before and after durability tests for the coatings prepared through different methods

| Method                 | WCA/WSA   | WCA/WSA after durability tests  | Ref.   |     |
|------------------------|---|---|--|-----|
| Spraying               | 168.6°  | CA > 150° (after the water impact test, sand impact test and tape-peeling test)<br>134° (after UV irradiation)<br>154° (after the anti-corrosion test)  | 87   |     |
|                        | 164.3 ± 3.2°  | 152.0 ± 2.5° (after the abrasion test)  | 81   |     |
|                        | CA > 150°/SA < 10°  | CA > 150° (after the anti-corrosion and laundering test)<br>CA > 150° (after the anti-corrosion test for 60 days)   | 102  |     |
|                        | 156°/4°   | CA > 140° (after the dynamic rotational oil-immersion test)<br>CA > 150°/SA < 10° (after the tape peeling test for 55 cycles and the anti-corrosion test)   | 103  |     |
|                        | CA > 150°/SA < 10°  | 136° (after the anti-corrosion test)  | 104  |     |
|                        | 156°/4°   | CA > 150° (after the sandpaper abrasion test, sand impact test and tape-peeling test for 50 cycles)<br>CA > 150° (after UV (30 W, 253.7 nm) irradiation for 12 h)<br>CA > 155° (after the anti-corrosion test for 12 h)<br>CA > 155° (after the high/low-temperature test at 180 °C/−10 °C for 12 h)                      | 105  |     |
|                        | (The CA and SA of <i>n</i> -hexadecane)<br>CA > 155°/SA < 10°   | (The CA of <i>n</i> -hexadecane)<br>CA > 150° (after the sandpaper abrasion test)<br>CA > 155° (after the tape-peeling test)<br>CA > 155°/SA < 7.5° (after UV (245 nm) irradiation for 24 h)<br>155° (after the anti-corrosion test for 60 min)<br>CA > 165°, SA < 5° (after the high/low-temperature test at −25–220 °C) | 106  |     |
|                        | CA > 150°/SA < 10°  | Receding CA, 155° (after the abrasion test for 10 cycles)<br>CA > 150° (after the stretch–release test for 3000 cycles)   | 107  |     |
|                        | 162.7°/2.7°   | CA > 145°/SA < 20° (after the water impact test at 50 kPa for 30 min)<br>156.6 ± 1.1°/6.8 ± 1.5° (after the anti-corrosion test for 1 h)<br>150.3°/25.4° (after the high/low-temperature test at 400 °C)<br>123.6° (after the high/low-temperature test at 450 °C)  | 126  |     |
|                        | 150°/5–17°<br>(The CA and SA of soybean oil) CA > 160°/SA < 10° | 150°/SA < 10° (after the sandpaper abrasion test)<br>151.6°/3.7° (after the Taber abrasion test for 21 cycles)<br>150.3°/25.1° (after the tape-peeling test for 150 cycles)<br>160.9°/7.3° (after the bending fatigue test for 500 cycles)  | 128<br>129   |     |
|                        | CVD   | 162°/0°   | 137.0°/1° (after the sandpaper abrasion test for 25 cycles)<br>CA > 150°/1.3° (after the tape-peeling test for 250 cycles)<br>CA > 162°/SA < 0.5° (after UV (365 nm, 3.7 mW cm <sup>−2</sup> ) irradiation for 72 h) | 121 |
|                        |   | 161°/4°   | 138° (after the sandpaper abrasion test)<br>CA > 150°/SA < 10° (after the tape-peeling test for 30 cycles)   | 123 |
|                        |   | 153°  | CA > 140°/SA > 30° (after the sandpaper abrasion test for 7 cycles)  | 47  |
| 165°/3°                |   | CA > 155°/SA < 8° (after the water impact test for 80 s)  | 112  |     |
| 168°                   |   | 161° (after the water impact test for 24 h)<br>156° (after the sand impact test for 120 s)<br>162° (after the anti-corrosion test in alkali for 12 days)<br>158° (after the anti-corrosion test in acid for 3 days)   | 110  |     |
| Sol-gel                |   | 165.7°  | CA > 150° (after the sandpaper abrasion test)<br>150° (after UV (16 W, 254–365 nm) irradiation for 18 days)<br>CA > 160° (after the anti-corrosion (pH = 2–12) test for 1 h)   | 43  |
|                        | 152°  | CA > 145° (after corrosion tests in alkaline and acid solutions)<br>CA > 120° (after the water impact test)   | 60   |     |
| Hydrothermal synthesis | 155°  | CA > 150° (after the water impact test for 480 min)   | 62   |     |
|                        | 152.9°  | CA > 150° (after UV (36 W, 356 nm) irradiation for 24 h)<br>CA > 150° (after the anti-corrosion test in 0.1 M hydrochloric acid (HCl) for one week)   | 53   |     |
|                        | 151 ± 3°/6 ± 3°   | CA > 150° (after the high/low-temperature test (boiling at 150 °C) for 10 h)<br>157°/20° (after the sandpaper abrasion test for 7 cycles)<br>155°/15° (after the tape abrasion test for 200 cycles)<br>154°/10° (after UV irradiation for 192 h)  | 56   |     |



Table 2 (Contd.)

| Method                 | WCA/WSA                                     | WCA/WSA after durability tests   | Ref. |
|------------------------|---|--|------|
| Graft copolymerization | 158°/4°                                     | CA > 150°/SA < 10° (after anti-corrosion testing in strong acid or alkali (pH = 4–12) for 24 h)                    | 58   |
|                        | 147°  | 157°/10° (after high/low-temperature testing at 140 °C)  |      |
|                        | Advancing CA of 159°<br>Receding CA of 155° | CA > 150° (after the anti-corrosion test, under ambient conditions for 3 months or pH = 12/pH = 2 for 2 h)         | 36   |
| Templating/<br>etching | 152.1°/7.4°                                 | 146° (after sandpaper abrasion test)   | 69   |
|                        |   | 140° (after the anti-corrosion (pH = 2, pH = 12) test)   |      |
|                        |   | 145° (under ambient conditions for 3 months)   | 37   |
|                        |   | CA > 150° (after the sandpaper abrasion test for 30 cycles, knife scratch test and finger wipe test for 50 cycles) |      |
|                        |   | CA > 150°/7.5° (after the anti-corrosion (pH = 1–13) test)   |      |
|                        |   | CA > 150°/SA < 8° (after the high/low-temperature test at 100 °C for 0.5 h)  |      |

2 and 3, and the factors other than measurements are outlined throughout this review.

### 3.1 Mechanical durability

We should note that there is still a lack of standardized test methods to systemically evaluate the mechanical durability of superhydrophobic surfaces. Most studies utilize homemade equipment that involve sand/water jet tests, rubbing the surfaces against sandpaper under a certain load, fast-peeling a high-tack tape from the surfaces, and rubbing with a pencil. No single measure has been used for characterizing the wear status. Different criteria including static contact angle, roll-off angle, *etc.*, have been used in the reported study. Therefore, we will provide the introduction of the measurement approaches and the mechanical durability evaluation in this section.

**3.1.1 Impact tests.** It is noteworthy that the sand impact and water impact tests are necessary for the superhydrophobic materials designed for outdoor applications. The impact tests are generally conducted under collisions with solid particles (sand) or liquid droplets (water). The surfaces of the materials should be placed at 45° from the horizontal plane. The collisions originate from the free falling of sand or water at a certain height and are triggered to destroy the surface topography of the superhydrophobic coatings. Herein, the detailed parameters of the impact device, the speed, and height of falling, the mass of sand or water, *etc.*, are specified in some standards for determining the abrasion resistance of coatings. For example, Deng *et al.* prepared a superhydrophobic coating of 25 nm thick silica shells coated with porous deposits of candle soot.<sup>80</sup> The coating presented the water contact angle (WCA) of 165° ± 1°. For the sand impact

Table 3 Summary of the parameters for impact tests

| Impact test     | Substrates   | Volume (μL)/<br>weight (g)  | Height (cm)/<br>speed (m s <sup>-1</sup> ) | Angle of sample to<br>horizontal (°) | Number of cycles/<br>time     | Ref. |
|-----------------|--|---|--|--------------------------------------|-------------------------------|------|
| Sand<br>impact  | Glass slides   | 30  | 50   | 45                                   | 120 s                         | 110  |
|                 | Glass slides/wood  | 10/30/50  | 50   | 45                                   | 30 s                          | 81   |
|                 | Glass slides   | 50  | 20   | 45                                   | 30 s                          | 87   |
|                 | Fabric   | 50  | 20   | —                                    | 50 times                      | 105  |
|                 | Slides, stainless steel  | 40  | 30   | —                                    | 60 min                        | 111  |
|                 | Glass slides   | 500   | 60   | 0                                    | 40 times                      | 106  |
| Water<br>impact | Glass slides   | 20  | 40   | 5                                    | 5 min                         | 80   |
|                 | Glass slides   | 100   | 30   | 45                                   | 5 times                       | 112  |
|                 | Glass slides   | 20 000  | 35   | 45                                   | 24 h                          | 110  |
|                 | Sponge, barbed wire,<br>plastic, cotton fabric,<br>wood, glass, A4 paper and<br>titanium plate | 22  | 50   | 30                                   | 5000 times                    | 81   |
|                 | Glass  | 22  | 50   | 45                                   | 5000 times                    | 87   |
|                 | Aluminium plate  | 25–50 (kPa)   | 20   | 45                                   | 30 min                        | 113  |
|                 | Aluminium plate  | 400 (kPa)   | 10   | Vertical                             | 30 min                        | 106  |
|                 | Glass  | Hexadecane drops with<br>a radius of 1 mm, water<br>drops of 1.3 mm | 1/10                                       | 45                                   | 360 000/12 000<br>water drops | 80   |
|                 | Glass slides   | 200 (kPa)   | 30   | 90                                   | 15 min                        | 109  |





tests, the gravel with a 100–300 mm diameter was dropped from a height of 10–40 cm to impact the coating with an energy of  $1 \times 10^{-8}$  to  $90 \times 10^{-8}$  J per grain. The  $\text{SiO}_2$  shell in the superhydrophobic coating was not strong enough to fully resist the grit impact, thus forming a crater at the impact site. However, if the coating thickness was kept above 2 mm as observed by scanning electron microscopy (SEM), the surface could maintain the original morphology with sub-micron roughness, that is, still retain superhydrophobicity.

Similarly, the superhydrophobic coatings based on various substrate surfaces were prepared with polydimethylsiloxane (PDMS) and polymethyl methacrylate (PMMA), as reported by Liu *et al.* Here, 10 g, 30 g and 50 g of sand particles with the size of approximately 300  $\mu\text{m}$  were applied to impact the PDMS/PMMA-coated surface by dropping them from a height of 50 cm for 30 seconds in a home-made setup as shown in Fig. 7a.<sup>81</sup> As shown by the results of WCA presented in Fig. 7e and f, different contact angles were obtained for different gravel weights after impact tests, but all maintained the superhydrophobic effect (WCA > 150°). The water impact test was applied to further evaluate the mechanical stability of the coatings by dropping approximately 5000 drops of water (approximately 22  $\mu\text{L}$  per drop) from a height of 50 cm in 2 h, and the modified setup is shown in Fig. 7b. The coating maintained a contact angle of 156.8° (Fig. 7h), demonstrating the continuous protection of the substrate. This can be ascribed to the retained nanoscale roughness after the impact tests, as supported by SEM images in Fig. 7c and d. Some studies performed the sand impact tests according to the ASTM D968-93 and ASTM D658-81(86) standards, which were provided for determining the abrasion resistance of organic

superhydrophobic coatings by the sand falling method and the sandblasting method, respectively. A representative summary of the recently reported parameters of impact tests based on different substrates is provided in Table 3.

**3.1.2 Sandpaper abrasion resistance tests.** In general, abrasion resistance is performed with linear abrasion, which requires a solid abradant, such as the reported rough sandpapers with different grades, SiC, rough paper (multi-hole and high compression paper wiper), *etc.*, to move tightly over to the tested superhydrophobic surfaces. Commercial superhydrophobic products must follow stringent industry requirements and standards, thus the mechanical durability should be judged by industry standards, such as the Tabor abrasion ASTM D4060, the Martindale method of abrasion, ASTM D4966, and AATCC standard, mainly for textile surfaces. The tests are commonly conducted using different instrumentation and test conditions.<sup>82</sup> However, there is still a lack of studies reporting compared adhesion performance concerning other studies. For example, different grades of sandpaper or other abradant materials with/without various weights of pressure have been used in the reported works to perform mechanical abrasion tests, and the related representative parameters are summarized in Table 4. Wang *et al.* reported that a wood-based biomimetic superhydrophobic surface with the size of 20 × 20 mm still maintained a contact angle greater than 150° after the sandpaper friction test.<sup>83</sup> As shown in Fig. 8a, the surface bearing a 50 g weight, was subjected to round-trip friction on a 1000 # sandpaper along the direction of a ruler. The WCAs decreased by approximately 3° in the case where the total friction distance was 200 cm. Zhang *et al.* carried out the test using a similar method, in

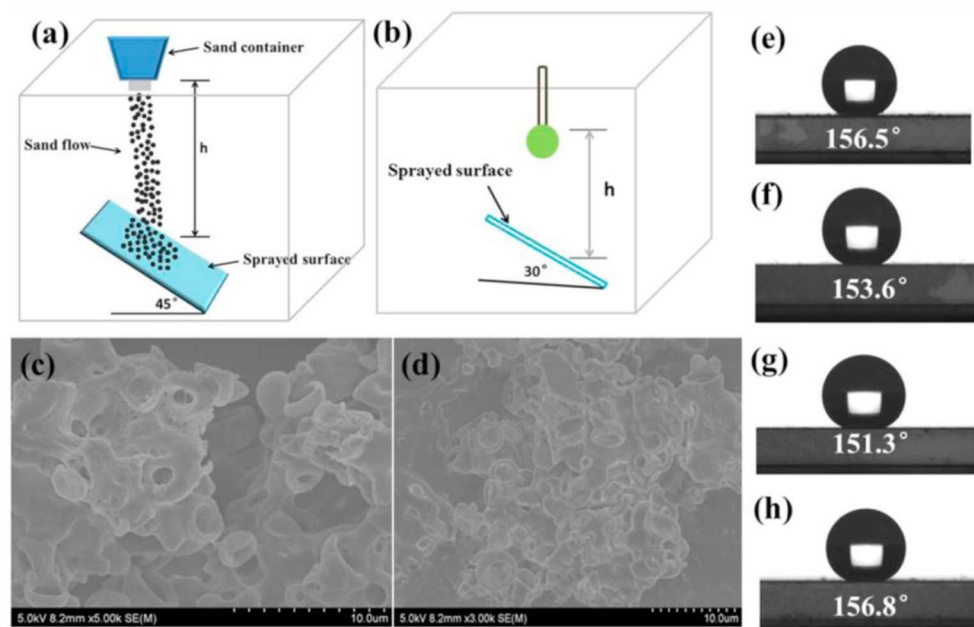


Fig. 7 Schematic diagram of the (a) sand impact abrasion test and (b) water droplet impact test. SEM images of the superhydrophobic surface after the (c) sand abrasion test and (d) water impact test. Contact angle profiles of superhydrophobic surfaces after (e) 10 g, (f) 30 g, and (g) 50 g of sand abrasion test and after (h) water impact test. Reproduced with permission from ref. 81. Copyright 2017, Elsevier.



Table 4 Summary of the parameters for sandpaper abrasion resistance tests

| Substrates                          | Sandpaper type                                  | Load (g)   | Rubbing distance in a single cycle (cm) | Cycles | Ref. |
|-------------------------------------|---|------------|---|--------|------|
| Sandpaper                           | SiC400 grit                                     | 100        | 20                                      | 50     | 114  |
| Solid-resin                         | SiC800 grid                                     | 200        | 40                                      | 10     | 115  |
| Wood                                | 1500 mesh                                       | 12.5 (kPa) | 30                                      | 10     | 74   |
| Fabric                              | SiC (800/1000/1200 mesh)                        | 100        | 30                                      | 40     | 116  |
| Fabric                              | 800 mesh  | 53         | 20                                      | 20     | 117  |
| Fabric                              | —   | 45 (kPa)   | —                                       | 300    | 118  |
| Nanofibres                          | —   | 20         | 5                                       | 100    | 119  |
| Fabric                              | —   | 50         | 2                                       | 50     | 120  |
| Glass                               | Micro-grained sandpaper (TUFBAK, ADALOX, P1000) | 100        | 20                                      | 25     | 121  |
| Glass                               | P1000   | 100        | 25                                      | 20     | 122  |
| Aluminium                           | 1000 mesh                                       | 5 (kPa)    | 60                                      | 1      | 123  |
| Wood                                | 1500 mesh                                       | 200        | 25                                      | 7      | 47   |
| Wood/glass                          | 600 mesh  | 100        | 10                                      | 12     | 103  |
| Wood/fabric                         | 1000 mesh                                       | 50         | 10                                      | 50     | 105  |
| Wood                                | Taber wear/800 cw                               | 100        | 5                                       | 30     | 106  |
| Glass slides/stainless steel plates | Friction tester (A20-339, MEIKO)                | 250        | —                                       | 550    | 111  |
| <i>Cis</i> -1,4-polyisoprene tape   | 1000 mesh                                       | 30         | 10                                      | 10     | 107  |
| Slides                              | 240 mesh  | 100        | 20                                      | 40     | 108  |
| Wood                                | 240 mesh  | 250        | 40                                      | 1      | 124  |
| MS plate                            | SiC/1200 mesh                                   | 50         | 16                                      | 20     | 125  |
| Wood                                | 800 mesh  | 200        | 10                                      | 8      | 43   |

which the superhydrophobic wood surface with the external load of 200 g (2 kPa), was moved on a 1500 mesh sandpaper for 25 cm (Fig. 8b).<sup>47</sup> It should be noted that the speed and direction of the object were manually determined by researchers and there were many other uncontrollable issues, such as the uneven abrasion caused by soft substrates (textile), the filling of the sandpaper gaps by the particles that fall off the coatings, *etc.*, which will affect the durability results, and therefore the standard parameters of the tests are still under debate. In this case, SEM tests are preferred to further analyze the extent of damage to the material caused by sandpaper abrasion during the sandpaper friction cycles by observing whether the rough structure of the surface has been destroyed (Fig. 8c).

**3.1.3 Tape-peeling tests.** For tape-peeling tests, a piece of tape with the highest adhesion strength is stuck onto the coating surface and pulled off; the process may be repeated

several times. Some reports recommend the use of the ASTM D3359 standard to conduct the test. For example, Milionis *et al.* assessed the adhesion effect of superhydrophobic surface coatings consisting of silicone rubbers based on aluminum substrates according to the ASTM D3359.<sup>84</sup> As shown in Fig. 9a, the tape was placed at 45° on the cross-shaded surface with the scratches to form chevrons or X-shaped scratch lines in the target area, and then peeled off after 1 min. The adhesion property of the coating was evaluated by the extent of damage as summarized in the indicative chart at the bottom of Fig. 9a. The results showed that there was no cracking or crumbling of the crossbeam square on the coating without silicone rubbers, and the adhesion test grade was 5B according to the ASTM D3359, while the cracking around the coating became obvious and the coating brittleness increased with the increase of the silicone rubber content. Likewise, for the superhydrophobic coatings based

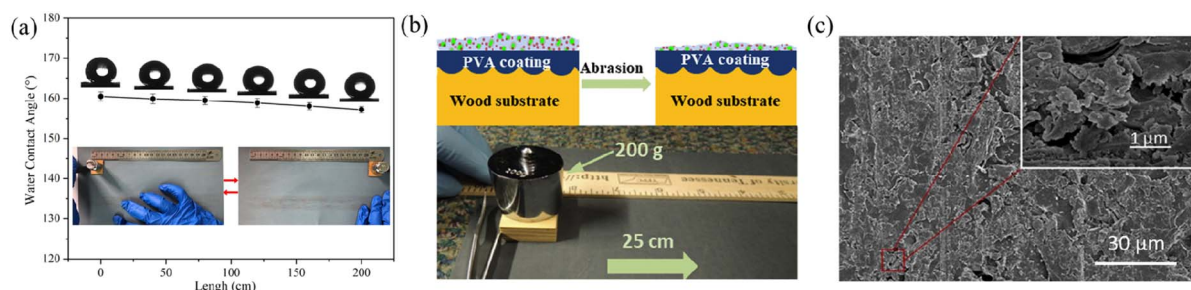


Fig. 8 (a) Schematic diagram of the sandpaper abrasion experiment, showing the effect of sandpaper abrasion length on the water contact angles of the superhydrophobic wood surface. Reproduced with permission from ref. 83. Copyright 2020, Elsevier. (b) Illustration of the damage of the PVA-coated wood surface induced by sandpaper abrasion and the photograph of the sandpaper abrasion test. (c) SEM images of the superhydrophobic wood surface after 6 cycles of abrasion. Reproduced with permission from ref. 47. Copyright 2018, Elsevier.



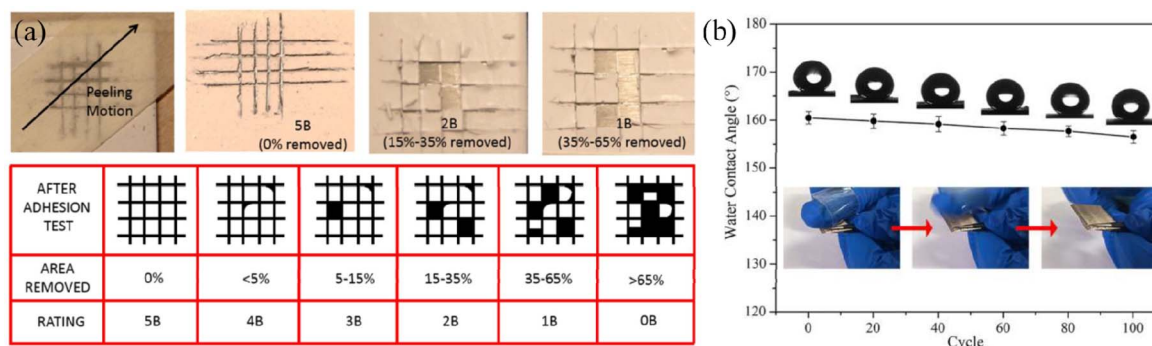


Fig. 9 (a) Schematic diagram of the tape peeling test for superhydrophobic coatings and the chart indicating the adhesion grade according to the ASTM D3359 standard. Reproduced with permission from ref. 84. Copyright 2015, Elsevier. (b) Illustration of the variation of water contact angles based on superhydrophobic coating with increasing tape peeling test cycles. Reproduced with permission from ref. 83. Copyright 2020, Elsevier.

on wood substrates, the tape peeling tests were performed by applying the highly adhesive tape with fingers to the superhydrophobic wood surface as reported by Wang *et al.* According to the results in Fig. 9a, the water contact angle exhibited an insignificant decrease from  $160.5^\circ$  to  $156.6^\circ$  after the 100 peeling cycles, indicating the durable mechanical property of the coating.<sup>83</sup> However, similar to the sandpaper adhesion tests, we should note that we could not provide precise judgment of mechanisms since the deposition of the tape adhesive on the coating and the removal of coating compositions by tape peeling easily occurred, and both will cause the decrease in hydrophobicity. Therefore, the tape peeling test has been considered as an additional measurement to evaluate the adhesion between the superhydrophobic coating and the substrate.

**3.1.4 Pencil hardness tests.** The pencil hardness test is another method for the assessment of the mechanical durability of superhydrophobic coatings. In the testing process, the pencil, with hardness ranging from 9B to 9H, is held in a carriage and placed at  $45^\circ$  from the coating surface and is moved tightly on the coating surface. For instance, Milonitis *et al.* performed a pencil hardness test for analyzing the mechanical durability properties of TEOS-treated silica coatings.<sup>84</sup> As shown in Fig. 10i, the pencil was fixed at  $45^\circ$  and performed 6.5 mm strokes at a speed of  $0.5 \text{ mm s}^{-1}$  on the film. The morphologies of the superhydrophobic coating after being damaged with different pencil hardness are presented in Fig. 10a–h, where the coating could withstand the pencil scratch with the hardness of 4H. Furthermore, the standards of ASTM D3363-2005 and GB/T 6793-1996 (China) are corresponding

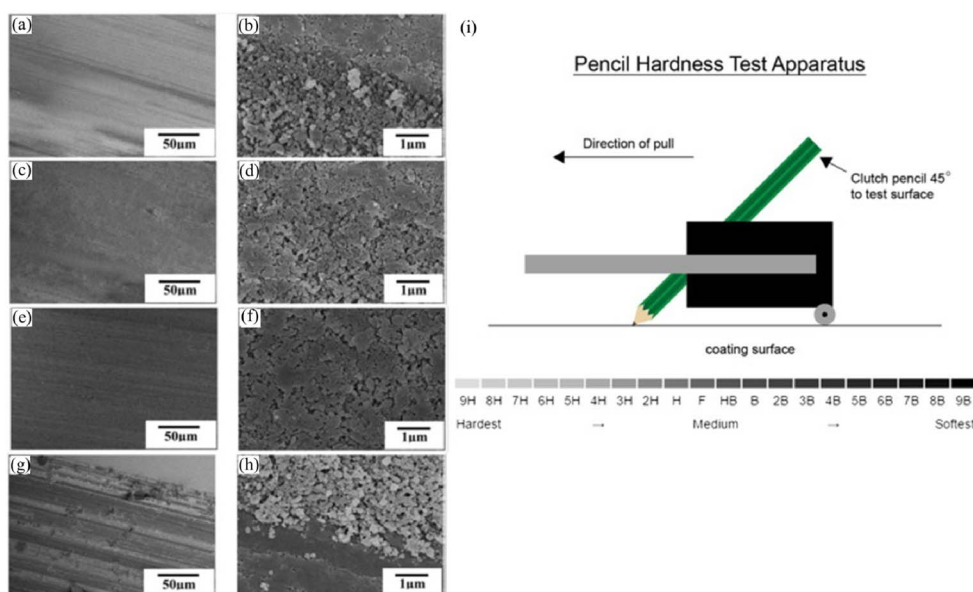


Fig. 10 SEM images of the as-prepared coatings after pencil scratch tests with different hardness: (a and b) 2H, (c and d) 3H, (e and f) 4H and (g and h) 5H. (i) Experimental setup for the pencil hardness test. Reproduced with permission from ref. 84. Copyright 2015, Elsevier.





provisions for pencil hardness tests, including the standards of pencil and eraser, as well as the standards of the substrates.

### 3.2 Chemical durability

The chemical stability of the material refers to the assessment of the superhydrophobic properties of the surface when exposed to corrosive liquids (*e.g.*, acidic/alkaline/salt solutions), UV irradiation, and so on. Generally, for the corrosion resistance tests, the coating is immersed for a certain duration in acidic, alkaline, or salty solutions with pH values ranging from 1 to 14. Another frequently reported test is using UV or sunlight irradiation to determine whether the coating is photo-resistant. After testing, the chemical durability is evaluated by the decreased degree of superhydrophobicity, which is caused by the degradation/decomposition of the hydrophobic constituents on the surface.

**3.2.1 Corrosion resistance tests.** Concerning corrosion resistance, the air layer on superhydrophobic coating plays an important role as a protective barrier, which can inhibit damage by surface corrosion and colonization.<sup>81</sup> Recently, Zhu *et al.* investigated the corrosion resistance of superhydrophobic glass in strong acids (HCl solution with pH = 2) and bases (NaOH solution with pH = 12) for 24 h.<sup>52</sup> The results showed that there was no significant reduction in the water contact angle and it remained above 150° after the tests. The corrosion rate of superhydrophobic coating decreased slightly due to its special microstructure, as proved by the microscopic morphology images. In the case of the superhydrophobic woodwork exposed to rain outside (commonly acidic) or other harsh environments, the chemical durability of the coatings strongly affects the water repellency of the products and causes damage to the physical and/or chemical properties of wood substrates. Of particular importance to the superhydrophobic wood is ensuring its adequate chemical stability before putting it into service. Wang *et al.* synthesized the  $\alpha$ -FeOOH film on the wood surface *via* a hydrothermal reaction and then modified the surface with octadecyltrichlorosilane (OTS) to obtain a superhydrophobic effect, thus achieving a highly corrosion-resistant superhydrophobic wood against both acid and alkali solutions.<sup>58</sup> In detail, the superhydrophobicity could be maintained after being immersed in sodium hydroxide solution at pH = 12 and hydrochloric acid solution at pH = 2 for 2 hours at room temperature, respectively.

**3.2.2 UV-resistance tests.** For man-made superhydrophobic surfaces, the water-repellent capability will gradually decrease due to the photodegradation of low-surface-energy agents under UV or sunlight irradiation. In this case, inorganic materials such as TiO<sub>2</sub>, ZnO, apatite, *etc.*, which are introduced to improve the roughness of coatings, can prohibit the degradation of coatings *via* oxidizing the contamination under photoirradiation; therefore, it is largely dependent on the inherent properties of the material components.<sup>82</sup> Recently, superhydrophobic coatings with adequate photo resistance have been considered promising products in practical applications. More importantly, wood has a wide range of applications in the furniture and construction markets, and the demand for

such applications makes it inevitable that wood products are exposed to sunlight radiation, in which irreversible aging damage will occur.<sup>85</sup> Li *et al.* fabricated the wood with TiO<sub>2</sub> (Ti-wood), TiO<sub>2</sub> and PDMS (Ti&P-wood), as well as in combination with electron beam treatment (R-Ti&P-wood) for comparing the water-repellent abilities and UV resistance properties of the as-prepared wood samples.<sup>43</sup> The accelerated UV aging tests were conducted for 18 days and the changes in surface appearance were recorded by photographs. After 18 days of UV exposure, the color of the original wood changed from white to yellow, while the surface of the R-Ti&P-wood did not change significantly (Fig. 11a and b), indicating that the superhydrophobic coating can resist discoloration under long-time irradiation. Similarly, the R-Ti&P-wood retained a contact angle of 159° after 18 days of exposure to UV light (Fig. 11c). From the results of UV-vis diffuse reflectance spectra (DRS) in Fig. 11d, it was found that the original wood showed a wide absorption in the range from 200 to 400 nm, illustrating that the original wood is susceptible to UV degradation. The absorption range of R-Ti&P-wood is smaller than that of the original wood but the maximum absorbance is still large (0.94); this may be due to the strong UV absorption ability of TiO<sub>2</sub>, thus the coating can effectively resist UV irradiation and prolong the service life of the wood.<sup>86</sup>

## 4. Emerging applications

Based on the previous discussion and the considerable number of reports, superhydrophobic wood plays a vital role in a large number of applications; however, its ability to be utilized is still restricted because the ambient temperature, humidity, *etc.*, can prevent the coatings from further preventing its destruction. Therefore, exploring and implementing novel functions such as anti-icing, oil-water separation, self-healing, triboelectric properties, and photothermal effects, *via* rational and effective strategies are pivotal but remain a challenge. In the following sections, we outline the recent works that report these functions to realize novel applications.

### 4.1 Photothermally-promoted anti-icing

Considering the intrinsic properties of wood, the woodwork used in the applications of outdoor buildings, gardens, trestles and beams, will suffer from freezing, ice accretion, or remaining wet for long periods in the winter or humid climates, which will pose serious challenges for wide practical applications. Generally, delaying the ice-formation time and temperature and increasing the melting rate of ice on the surfaces could reduce the risk of warping and cracking of wood, thus extending its service life. Herein, the delay time ( $\Delta t$ ) was calculated by  $\Delta t = t^* - t_0$ , where  $t^*$  is the time taken to start freezing and  $t_0$  is the time taken to reach 0 °C.<sup>87</sup>

More recently, Cao *et al.* reported a superhydrophobic wood with repellent abilities toward five kinds of liquid (milk, soy sauce, juice, and coffee), excellent mechanical durability, and anti-icing property, which was fabricated by SiO<sub>2</sub> sol and poly(methylhydrogen)siloxane (PMHS).<sup>88</sup> Concerning the anti-icing test, the wood with the superhydrophobic properties was



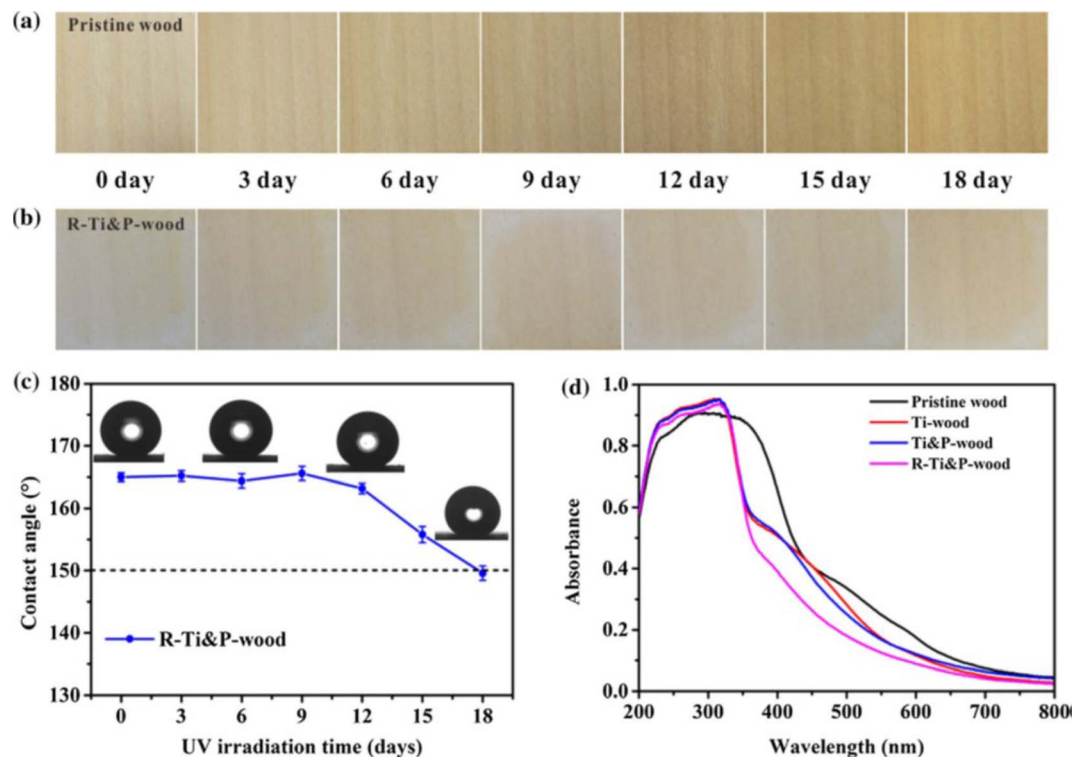


Fig. 11 Photographs of (a) pristine wood and (b) R-Ti&P-wood within 18 days of UV irradiation (taken every three days). (c) The contact angle change of R-Ti&P-wood as a function of UV irradiation time. (d) UV-vis diffuse reflectance spectra (DRS) of pristine wood, Ti-wood, Ti&P-wood and R-Ti&P-wood. Reproduced with permission from ref. 43. Copyright 2021, Springer Netherlands.

immersed in water and placed under freezing conditions at  $-20\text{ }^{\circ}\text{C}$  for 24 h, then removed and allowed to melt at room temperature. As a result, the wood surface maintained the superhydrophobicity with a contact angle larger than  $150^{\circ}$ . Wu *et al.* produced a transparent, anti-icing, bio-based epoxy coating on wood surfaces.<sup>89</sup> The coating exhibited superior water repellency and a delayed icing time of 165 s at  $-15\text{ }^{\circ}\text{C}$ , and no residual ice could be found on the coated wood surfaces. The anti-icing properties can be ascribed to the apparent surface energy and the highest magnitudes of surface roughness contributed by the 3D convex-concave microstructure.

It has also been found that wood with a photothermal effect can self-melt the surficial ice by photo-to-thermal conversion under sunlight irradiation, which is an environmentally-friendly and efficient strategy for achieving self-cleaning and anti-icing effects. Interestingly, inspired by the optical features of the moth's eye, Zhao *et al.* prepared the coating with a biomimetic protrusion array on the surface of the aluminum substrate by ultrafast laser texturing technology, in which the moth-eye bionic structure was extremely pivotal for capturing more incident light, allowing multiple reflections and thus converting more heat (Fig. 12a).<sup>90</sup> Compared with bare aluminum and bionic hydrophilic aluminum, bionic superhydrophobic aluminum enabled the most rapid increase in surface temperature in the same period (Fig. 12e), further proving the remarkable photothermal effect of the bionic superhydrophobic coating. As shown in Fig. 12b-d, the heat

produced by photothermal ability promoted the ice melting on the superhydrophobic surface within the relatively shortest time (4 min), while the residual ice remained on the surfaces of the other two samples. The integrated superhydrophobic property and photothermal effect synergistically boosted the anti-icing performance and endowed it with self-cleaning ability.

#### 4.2 Photothermally-enhanced oil-water separation

As a natural, porous material, the superhydrophobic wood-based sponge material, different from ordinary aerogels, has high elasticity, re-compressibility, stretchability, and adsorption due to its unique structure. However, the high viscosity of oil restricts the highly efficient absorption of wood microchannels, thus preventing it from reaching the highest saturation. Recently, the photothermal effect has been found to effectively improve the efficiency of oil-water separation, oil collection, and seawater desalination by decreasing the viscosity of oil with increasing temperature. For example, Gao *et al.* fabricated a superhydrophobic wood-based elastomer *via* the chemothermal method.<sup>91</sup> Superhydrophobicity with the WCA of  $152^{\circ}$  was achieved by tuning the multi-structure of wood using polysaccharide degradation, which tailored the cellulose nanoarrays and removed the hydrophilic groups from the lignin. It was also found that the aromatic skeleton of the residual lignin exhibited excellent photo-to-thermal conversion ability (temperature increased to  $83\text{ }^{\circ}\text{C}$ ). The superhydrophobic lumen of wood enabled the oil-water separation property with



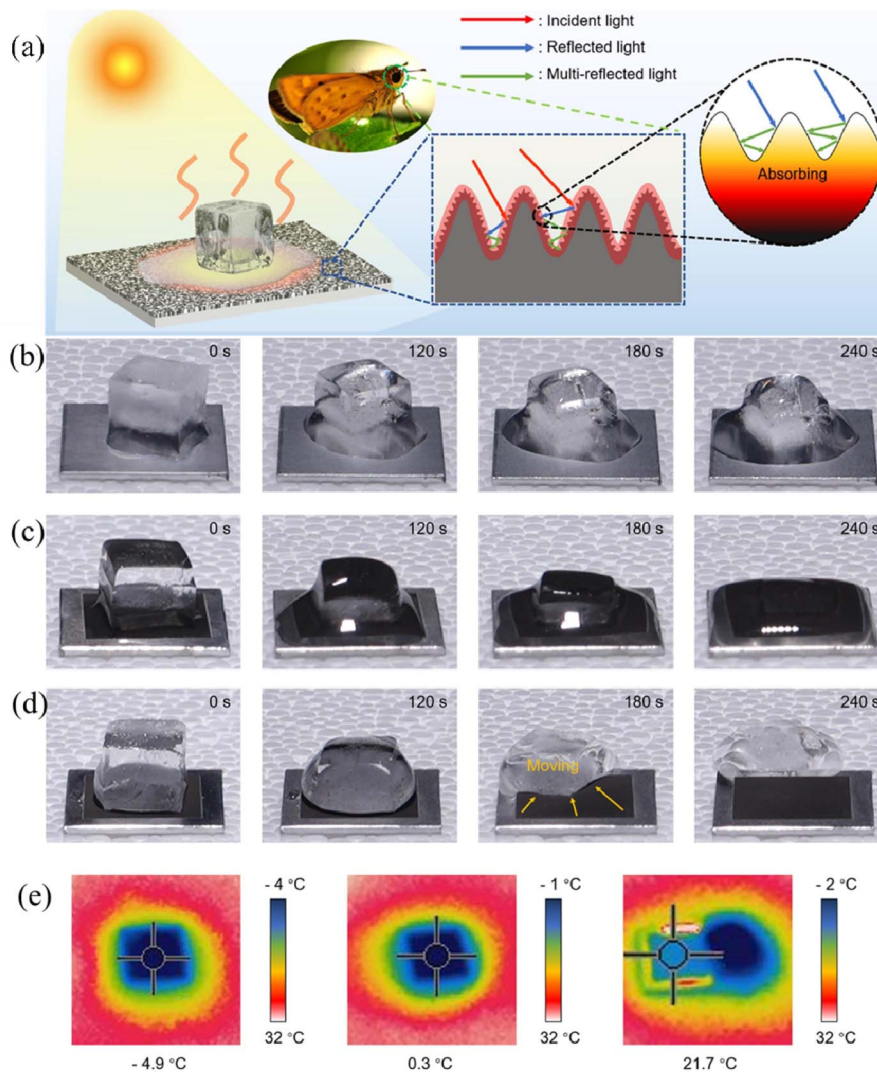


Fig. 12 (a) Schematic illustration of the anti-icing process of the moth-eye-inspired texturing surfaces (MTS) under solar irradiation. The solar-thermal energy conversion efficiency is enhanced by multiple internal reflections induced by the dual-scale microstructure. Photographs of the ice melting on different surfaces with/without photothermally-promoted anti-icing, including (b) ordinary smooth aluminum, (c) bionic hydrophilic aluminum, and (d) bionic superhydrophobic aluminum with one sun irradiation. (e) The infrared thermal images of smooth aluminum, bionic hydrophilic aluminum, and bionic superhydrophobic aluminum at 270 s. Reproduced with permission from ref. 90. Copyright 2021, Elsevier.

absorption capacities ranging from 12 to 22.7 g g<sup>-1</sup> for different kinds of oil (Fig. 13a). As is well known, elevating the temperature could promote oil mobility during the absorption process. Therefore, the *in situ* thermal effect produced by photothermal conversion in the wood elastomer greatly reduced the oil viscosity by two magnitudes (54 mPa s) and boosted the oil filling into the elastomer, resulting in a high oil collection rate of 8 L h<sup>-1</sup> g<sup>-1</sup> within 160 s. In another work, the superhydrophobic wood (PDMS@GSH wood) possessing both Joule heat and the photothermal effect was fabricated with reduced graphene oxide (GSH) and vinyl-terminated polydimethylsiloxane (V-PDMS), as reported by Chen *et al.*<sup>92</sup> The GSH contributed the heat with the surface temperature up to 139 °C, which was produced by integrated electrothermal (Joule heat) and photothermal effects (Fig. 13c). This led to an improved crude oil–water separation rate of 1.78 × 10<sup>5</sup> kg m<sup>-3</sup>

for PDMS@GSH wood under sunlight in comparison to the delignified wood without sunlight irradiation, which suggests the potential for saving the energy of crude oil clean-up (Fig. 13b). Likewise, Wang *et al.* prepared the polydimethylsiloxane@wood sponge/MXene (PDMS@WSM), which has advantages of adsorbing crude oil with the maximum capacity of 11.2 × 10<sup>5</sup> g m<sup>3</sup> in 6 min and continuously collecting 25 ml of crude oil in 150 s.<sup>93</sup> This was ascribed to the porous and compressible structure, and the hydrophobic and lipophilic high-efficiency adsorbent promoted by Joule heat and photothermal conversion effects (Fig. 13d).

#### 4.3 Photothermally-induced smart self-healing performance

Inspired by the observation that most organisms can repair themselves after being damaged, constructing materials with





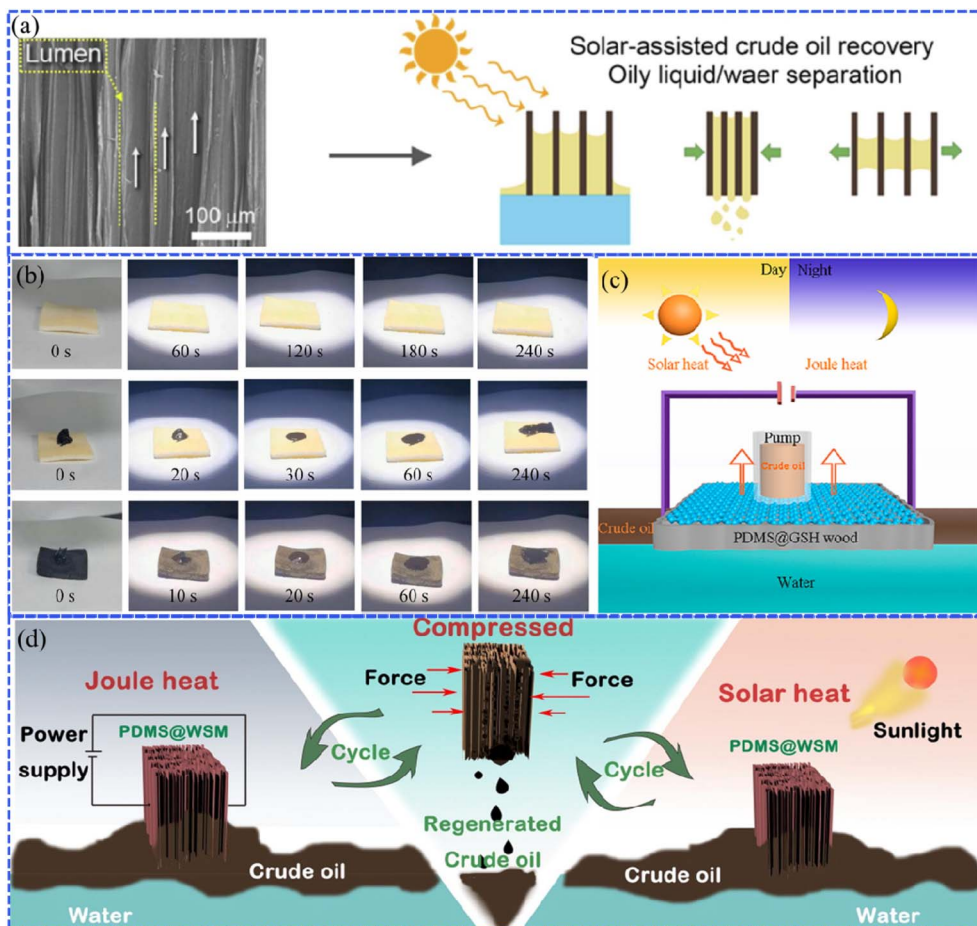


Fig. 13 (a) Schematic illustration of the absorption-squeezing recovery of oil based on the wood elastomer. Reproduced with permission from ref. 91. Copyright 2022, Elsevier. (b) Photographs illustrating the changes in oil adsorption for different wood samples within 240 s, including delignified wood, delignified wood with crude oil, and PDMS@GSH wood with crude oil under sunlight. Reproduced with permission from ref. 92. Copyright 2023, Elsevier. (c) Schematic illustration of the cleaning-up process of crude oil based on PDMS@GSH wood. Reproduced with permission from ref. 92. Copyright 2023, Elsevier. (d) Diagram of Joule heating and solar heating PDMS@WSM for cleaning up and recovering viscous crude oil spills. Reproduced with permission from ref. 93. Copyright 2022, Elsevier.

self-repairing properties has attracted lots of attention. This so-called self-healing behavior, which can effectively prolong the service life and stability of materials, as well as avoid excessive maintenance costs, is especially important for artificial superhydrophobic coatings. The strategies for achieving the self-healing function can be classified into three categories. One is to embed the roughness-shaping and low-surface-energy constituents into polymer films, heterogeneous interpenetrated networks, or porous matrices. Then, the hydrophobic components would migrate to the damaged area under the external stimuli, thus playing a self-healing role.<sup>24</sup> The other is to construct a hierarchical microstructure, of which a surface with dual-scale roughness is created through a layer-by-layer deposition process. For example, the researchers embedded the hydrophobically-modified silica particles into the fluorinated polymer matrix to prepare the superhydrophobic surface. When the surface was damaged during abrasion tests, the embedded hydrophobic silica particles were exposed and created a new rough surface, resulting in a regenerated superhydrophobic surface due to the effect of the roughness-

regenerating capability.<sup>21</sup> The last category is to fabricate self-healing superhydrophobic coatings using supramolecular polymers, which possess reversible dynamic bonds, such as multivalent hydrogen bonds and disulfide bonds. The strong bonding between the substrates and superhydrophobic coatings provides high shear strength and stable mechanical strength, and the superhydrophobic properties can be recovered by heating or other stimuli.<sup>94</sup> However, there are still some problems to solve in the field of self-healing superhydrophobic materials. For example, the coating should be soft enough to satisfy the mobility of chemical migration, but it is difficult for such a soft coating to achieve surface roughness regeneration on the substrates. Therefore, low surface energy may not be achieved on such topographic structures. Besides, it is tough to achieve completely invisible defects on the coatings if one only depends on self-healing without any other stimulus, even after a long period. Generally, the external stimulus using water, heat, light or plasma treatment is the common means to improve the healing efficiency and reduce the responsive time



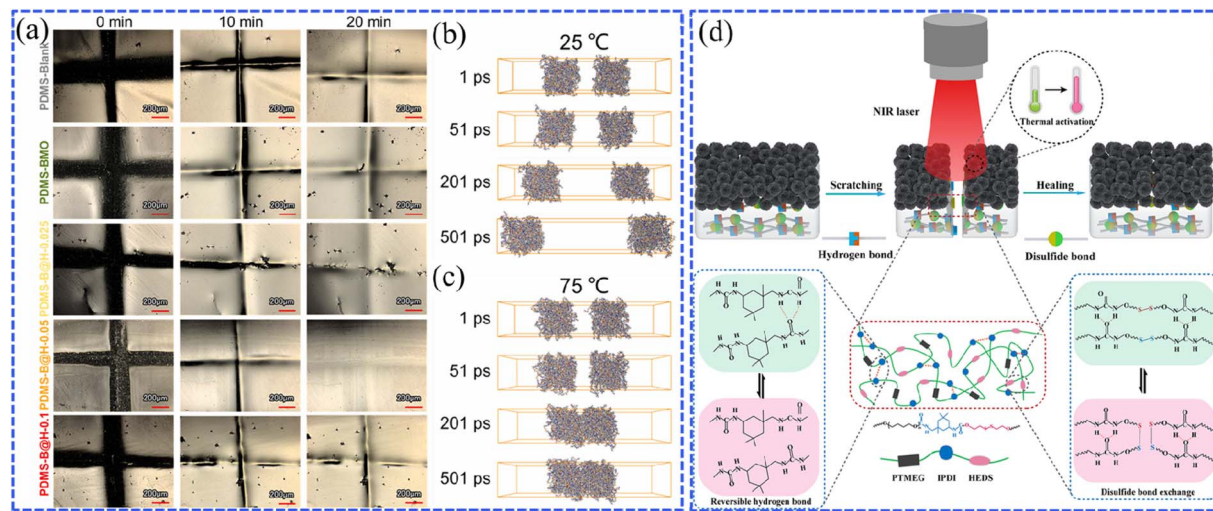


Fig. 14 (a) Photographs showing the self-healing process of PDMS–Bi<sub>2</sub>MoO<sub>6</sub>@HTCC with different amounts of HTCC within 20 min. The self-healing motion trajectories of PDMS (b) at 25 °C and (c) 75 °C. Reproduced with permission from ref. 95. Copyright 2022, Elsevier. (d) Schematic illustration of the self-healing mechanism of the polyurethane/ZnO@polydopamine-stearic acid (PU/ZnO@PDA-SA) coating. Reproduced with permission from ref. 96. Copyright 2022, American Chemical Society.

of self-healing materials, thus some limitations exist in practical applications.<sup>24</sup>

Recently, photothermally-induced self-healing materials have been widely studied since photo-to-thermal conversion is a convenient and economical way to obtain thermal energy. For instance, Wang *et al.* designed a tunable photothermal self-healing coating composed of Bi<sub>2</sub>MoO<sub>6</sub>, hydrothermal carbonation carbon (HTCC), and PDMS (PDMS–Bi<sub>2</sub>MoO<sub>6</sub>@HTCC).<sup>95</sup> As the results of the scratch and illumination tests show in Fig. 14a, the self-healing efficiency of the optimized PDMS–Bi<sub>2</sub>MoO<sub>6</sub>@HTCC (the precursor of HTCC is 0.05 g) coating reached 92.71% after 20 min of illumination. This is because the larger amount of heat generated in HTCC (~75 °C, Fig. 14b and c) promoted the breaking and reconstruction of the dynamic bonds (hydrogen bonds), leading to the recovery of PDMS chains. Li *et al.* prepared multifunctional superhydrophobic coatings that possessed room-temperature stability, mechanical stability, self-healing properties, and near-infrared light stimulation responses.<sup>96</sup> The self-healing polyurethane (PU) grafted with long-chain aliphatic stearic acid (SA) was used as the interfacial reinforcement layer, while the poly(dopamine) (PDA)-coated flower-like ZnO composite particles were synthesized to form the hydrophobic layer. The dynamic hydrogen and disulfide bonds in PU enabled the self-healing performance, while the PDA with near-infrared responsibility created the rapid self-healing ability (Fig. 14d). However, a thorough investigation of the intrinsic role of the photothermal effect is required, especially in the dynamic bond reconstruction during the self-healing process. Meanwhile, as a resource-sustainable material, such self-healing superhydrophobic wood-based materials should be seriously considered to increase the high value-added use of wood and protect precious wood resources. It requires a rational molecular design to not only intensify the mechanical strength of

superhydrophobic coatings,<sup>97</sup> but also to rehabilitate them from damage and preserve their mechanical properties.

#### 4.4 Wettability-controllable wood-based materials for energy storage and conversion

**4.4.1 Wood-based nanogenerators.** Wood is an anisotropic material with high structural strength in the direction of fiber growth. The crystalline regions of cellulose in the wood contribute a certain triboelectric effect when subjected to mechanical vibrations and some other stimuli, which makes it a promising electrode material for nanogenerator applications.<sup>98,99</sup> The triboelectric effect can be enhanced by chemical treatments, such as delignification, and composited with other triboelectric materials, *etc.* Although these means can significantly increase the triboelectric constant and electrical output properties of wood, they will also create negative effects on the mechanical strength. As is well known, owing to the simple contact power generation and the small size, triboelectric nanogenerators (TENGs) have been extensively applied in the fields of stretchable, wearable, shape-adaptive, and other energy devices. The unstable mechanical strength of the wood nanogenerators causes them to withstand severe deformation, directly limiting the development of wood-based electronic devices. Luckily, most of the polymers used in superhydrophobic coatings, such as polydimethylsiloxane (PDMS), polyurethane (PU), and so on, are triboelectric materials. Therefore, the innovative application of superhydrophobic wood in nanogenerators will greatly strengthen the mechanical and chemical durability and the electrical output performance of the devices. For example, Li *et al.* fabricated an integrated flexible superhydrophobic self-charging device consisting of a multi-operating mode TENG (MTENG) and an all-solid-state micro-supercapacitor (MSC) by mimicking the water-repellent surface of the lotus leaf and laser-induced graphene (LIG)





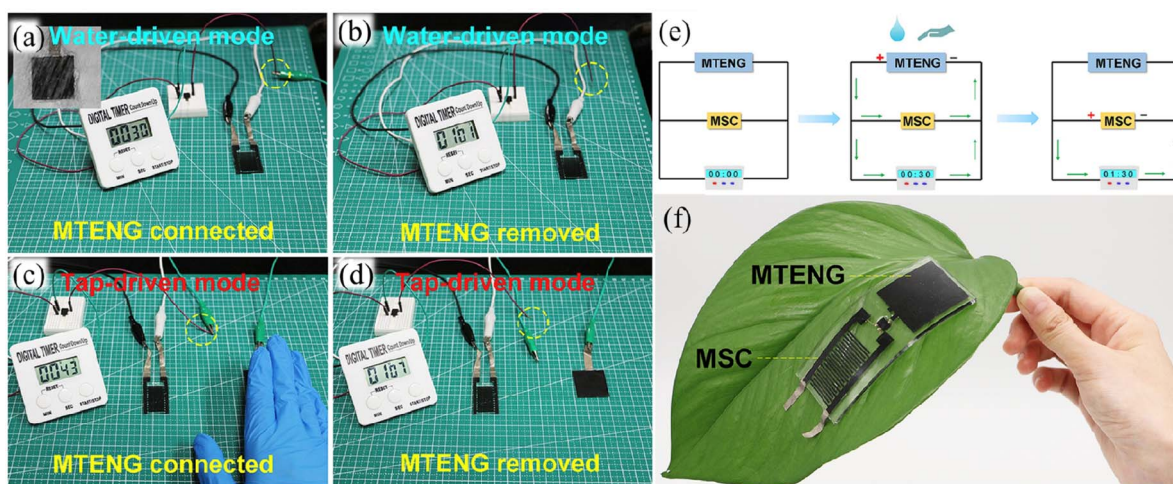


Fig. 15 Schematic illustration of MSC and a timer working in (a) the water-driven mode charged by MTENG, (b) the water-driven mode after removing MTENG, (c) the tap-driven mode charged by MTENG, and (d) the tap-driven mode after removing MTENG. (e) Illustration of the operating mechanism of MTENG and MSC. (f) Photograph of the MTENG and MSC devices attached to the leaf. Reproduced with permission from ref. 100. Copyright 2020, Elsevier.

technology.<sup>100</sup> The MTENG can be driven in two modes, that is, hand-touching (Fig. 15a and b) and water-dropping (Fig. 15c and d). In the two operation modes (Fig. 15e), the MTENG can charge both the small timer and the MSC. The superhydrophobic surface with the lotus leaf-like bionic structure endowed the device with self-cleaning properties and ensured its normal operation under humid conditions. More interestingly, the authors found that when attaching the device to the crop leaf surface with double-sided tape (Fig. 15f), the device could collect and convert the triboelectric energy produced by leaf vibrations and falling raindrops.

**4.4.2 Wood-based electrode materials.** The orderly pore channels of wood cell walls provide nutrients for sustaining life and also supply structural support for tri-phase (solid, liquid, gas) interfaces. Wood contains a large amount of carbon, which provides an adequate source of carbon during pyrolysis. Highly conductive graphitized carbon is formed during the elevated carbonization, which would accelerate the transfer of electrons during the reactions of energy storage and conversion. With the above advantages, wood has huge potential in the design and manufacture of electrocatalytic materials with high catalytic reactivity and controllable wettability. For instance, Liao *et al.* devised a wood-derived integrated electrocatalytic electrode (Ni/CW) with tailored surface wettability for the urea oxidation reaction (UOR).<sup>130</sup> The wood electrode showed tunable superhydrophilic/superaerophobic surface characteristics due to the embedded and evenly distributed papillary nickel nanoparticles in the inner wall of the pore channels in the wood. This leads to superior UOR catalytic performance in alkaline electrolytes. The superwetting capabilities of wood-based electrodes assure continuous interactions between the active site and electrolyte, while the produced gases are accelerated to escape, resulting in the boosting of the mass transfer and electrocatalytic reactions. Such wood-based materials with controllable wettability have shed new light on the rational design and configuration of electrocatalytic electrodes.

## 5. Conclusion and outlook

In recent years, great efforts have been devoted to constructing robust biomimetic superhydrophobic coatings on wood surfaces, with many studies utilizing the advances in preparation methods and durability tests. Inspired by naturally existing superhydrophobic phenomena such as the famous 'lotus effect', many synthetic strategies have been developed to rationally design the microstructures and chemical surface energies of artificial superhydrophobic surfaces. In addition, according to the comprehensive understanding of the relationship between the air layer and substrate surface, the mechanisms of superhydrophobic durability, including mechanical abrasions and chemical decays, have been uncovered. Particularly, with the development of modern characterization techniques, information on coating damage can be obtained, thus optimizing the superhydrophobic coating in accordance with different theories. Notably, representative emerging applications, where the water-repellent abilities of wood-based products become crucial, were discussed. As noted above, great progress has been made regarding the synthesis routes to superhydrophobic coatings that are suitable for modifying wood substrates, the techniques for evaluating durability, and the new applications. However, considerable challenges remain that will enrich the existing research for the future development of superhydrophobic wood as outlined in the following.

(1) Practical modification technologies are required to yield superhydrophobic wood. In general, superhydrophobic modification is a type of surficial treatment that occurs on the surface of substrates. Therefore, the water-repellent and durability performances are largely dependent on the thickness of the superhydrophobic coating. In this context, the surface roughness (such as the overhanging micro and nanostructure, concave-convex nanostructure, *etc.*) should be introduced to the substrates by chemical bonds, especially covalent bonds, thus



improving the adhesion between the coatings and substrates. Moreover, simple, low-cost, environmentally friendly and harmless preparation methods, such as dipping, spraying, *etc.*, should be further developed to facilitate the industrial production and application of superhydrophobic woodwork.

(2) The transparency of superhydrophobic coatings should be further considered for wood substrates. This is especially important for woodwork applied in some special applications that require the wood to maintain its natural color and texture. However, most of the agents used to achieve roughness and low surface energy tend to cause color changes due to the chemical reactions occurring between the agents and wood substrates. Moreover, a rough geometry tailored by nanomaterials with a more complex morphology is highly desirable in order to achieve the optimized distribution of the air layer and superhydrophobic coating with high transparency. In this context, particular efforts should be made to precisely predict the coating performance, including superhydrophobicity, stability, and real-life service time by theoretical modeling and calculations based on their irregular microstructure. Therefore, it remains a tremendous challenge to further explore the relationship between the superhydrophobicity and the transparency of coatings.

(3) A comprehensive standard system is imperative for the evaluation and comparison of the durability of superhydrophobic coatings. Since there are no unified test methods including testing conditions and evaluation standards for comparing the artificial superhydrophobic coatings, the corresponding experimental results cannot provide sufficient accuracy to confidently apply the as-prepared products in real-world applications. Moreover, some additional techniques for morphological characterization (*e.g.*, scanning electron microscopy, SEM) and chemical composition analysis (Fourier transform infrared spectroscopy, FTIR) to investigate the growth process of superhydrophobic coatings, have been used to assess the performance. However, learning from the self-organization of organisms, which precisely engineered the functional surfaces with significant superhydrophobic effects, the characterization methods could be scaled up to capture the real-world dynamic construction of artificial superhydrophobicity, which will influence the rational design of robust superhydrophobic woodwork. For instance, *in situ* SEM, Raman, FTIR, WCA tests, *etc.*, should be developed for the real-time monitoring of the interface evolution, which will greatly progress the field of superhydrophobic materials.

(4) There is substantial room for developing superhydrophobic wood with new functionalities to expand the scope of its applications. Some new applications have been demonstrated to enable the various combinations of functionalities, including self-healing, oil-water separation, anti-icing, triboelectric properties, photothermal effects and electrocatalytic activities. Conversely, applying superhydrophobic technology to the above applications is of great economic significance for overcoming the issues of mechanical damage, including deformation, warping, cracking, *etc.* The coating materials (*e.g.*, PDMS<sup>31</sup>) that act as both the superhydrophobic agent and functional materials with triboelectric properties should be

developed, and the mechanism that leads to collective properties should be comprehensively investigated to further develop robust and low-cost superhydrophobic wood.

(5) More available fields should be further explored to extend the emerging engineering applications of superhydrophobic wood. Advanced wood processing technology poses considerable challenges for the wood industry. Moldable wood, transparent wood, magnetic wood, *etc.*, have attracted considerable attention because of their special functional features. Inspired by these materials, superhydrophobic wood with single-, dual-, or multi-functions such as thermal conduction, electric conduction, magnetic properties, light absorption, luminescence properties, *etc.*, will be more desirable in multiple domains, such as the anti-icing of wooden plank roads, boat decks for water operations, interior decoration materials for rail transit and other applications in furniture, construction, transportation, and new smart materials of energy storage and conversion.

New opportunities to explore superhydrophobic wood for use in emerging applications are abundant. The standardized evaluation system for tracking the durability, clarifying the actual preparation, unveiling the superhydrophobic mechanism, and rationally designing the superhydrophobic wood should be further developed. We anticipate that this review will provide a comprehensive source of information to propel the future advancement of superhydrophobic wood.

## Conflicts of interest

There are no conflicts to declare.

## Acknowledgements

This work was financially supported by the Natural Science Foundation of Heilongjiang Province (YQ2022C001), China Postdoctoral Science Foundation funded project (2022M710645), and the Fundamental Research Funds for the Central Universities (2572022BB03).

## References

- 1 W. Weng, M. Tenjimbayashi, W. H. Hu and M. Naito, *Small*, 2022, **18**, 2200349.
- 2 C. Schlaich, M. Li, C. Cheng, I. S. Donskyi, L. Yu, G. Song, E. Osorio, Q. Wei and R. Haag, *Adv. Mater. Interfaces*, 2022, **5**, 1701254.
- 3 W. Wang, H. Lai, Z. Cheng, Z. Fan, D. Zhang, J. Wang, S. Yu, Z. Xie and Y. Liu, *ACS Appl. Mater. Interfaces*, 2020, **12**, 49219–49226.
- 4 X. Wang, L. Dai, N. Jiao, S. Tung and L. Liu, *Chem. Eng. J.*, 2021, **422**, 129394.
- 5 L. Wang, S. Zhang, S. Li, S. Yan and S. Dong, *R. Soc. Open Sci.*, 2020, **7**, 200066.
- 6 W. Barthlott and C. Neinhuis, *Planta*, 1997, **202**, 1–8.
- 7 P. Liu, X. Bai, W. Xing, Y. Zhang, N. Chen, Y. Zhang, L. Qu and J. Ma, *Mater. Chem. Phys.*, 2021, **259**, 124049.





- 8 S. Zhou, X. Zhu and Q. Yan, *Surf. Interface Anal.*, 2018, **50**, 290–296.
- 9 N. Wang, Q. Wang, S. Xu and L. Lei, *J. Cleaner Prod.*, 2021, **312**, 127836.
- 10 Y. Wang, Z. Tang, S. Lu, M. Zhang, K. Liu, H. Xiao, L. Huang, L. Chen, H. Wu and Y. Ni, *Holzforschung*, 2020, **74**, 799–809.
- 11 R. Zhang, J. Wei, N. Tian, W. Liang and J. Zhang, *ACS Appl. Mater. Interfaces*, 2022, **14**, 49047–49058.
- 12 J. Wei, B. Li, N. Tian, J. Zhang, W. Liang and J. Zhang, *Adv. Funct. Mater.*, 2022, **32**, 2206014.
- 13 H. Xie, J. Wei, S. Duan, Q. Zhu, Y. Yang, K. Chen, J. Zhang, L. Li and J. Zhang, *Chem. Eng. J.*, 2022, **428**, 132585.
- 14 J. Wei, B. Li, L. Jing, N. Tian, X. Zhao and J. Zhang, *Chem. Eng. J.*, 2020, **390**, 124562.
- 15 X. Zhao, J. Wei, B. Li, S. Li, N. Tian, L. Jing and J. Zhang, *J. Colloid Interface Sci.*, 2020, **575**, 140–149.
- 16 Y. Yang, B. Li, L. Li, S. Seeger and J. Zhang, *iScience*, 2019, **16**, 420–432.
- 17 H. Zhang, X. Bu, W. Li, M. Cui, X. Ji, F. Tao, L. Gai, H. Jiang, L. Liu and Z. Wang, *Adv. Mater.*, 2022, **34**, 2203792.
- 18 D. Wang, Q. Sun, M. J. Hokkanen, C. Zhang, F. Y. Lin, Q. Liu, S. P. Zhu, T. Zhou, Q. Chang, B. He, Q. Zhou, L. Chen, Z. Wang, R. H. A. Ras and X. Deng, *Nature*, 2020, **582**, 55–59.
- 19 Y. Li, W. Ma, Y. S. Kwon, W. Li, S. Yao and B. Huang, *Adv. Funct. Mater.*, 2022, **32**, 2113297.
- 20 K. Ellinas, A. Tserepi and E. Gogolides, *Adv. Colloid Interface Sci.*, 2017, **250**, 132–157.
- 21 T. Verho, C. Bower, P. Andrew, S. Franssila, O. Ikkala and R. H. A. Ras, *Adv. Mater.*, 2011, **23**, 673–678.
- 22 J. Jeevahan, M. Chandrasekaran, G. B. Joseph, R. B. Durairaj and G. Mageshwaran, *J. Coat. Technol. Res.*, 2017, **15**, 231–250.
- 23 H. Y. Erbil, *Langmuir*, 2020, **36**, 2493–2509.
- 24 Y. Qing, S. Shi, C. Lv and Q. Zheng, *Adv. Funct. Mater.*, 2020, **30**, 1910665.
- 25 Y. Tan, K. Wang, Y. Dong, S. Gong, S. Shi and J. Li, *Chem. Eng. J.*, 2022, **448**, 137487.
- 26 Y. Zhao, D. Qu, T. Yu, X. Xie, C. He, D. Ge and L. Yang, *Chem. Eng. J.*, 2020, **385**, 123860.
- 27 C. Chen, Y. Wang, Q. Wu, Z. Wan, D. Li and Y. Jin, *Chem. Eng. J.*, 2020, **400**, 125876.
- 28 W. Zhao, L. Xiao, X. He, Z. Cui, J. Fang, C. Zhang, X. Li, G. Li, L. Zhang and Y. Zhang, *Opt. Laser Technol.*, 2021, **141**, 107115.
- 29 T. Wang, W. Wang, H. Feng, T. Sun, C. Ma, L. Cao, X. Qin, Y. Lei, J. Piao and C. Feng, *Chem. Eng. J.*, 2022, **446**, 137077.
- 30 S. Zhang, X. Huang, D. Dong, W. Xiao, L. Huo, M. Zhao, L. Wang and J. Gao, *ACS Appl. Mater. Interfaces*, 2020, **12**, 47076–47089.
- 31 J. Luo, M. Zhang, B. Yang, G. Liu, J. Tian, J. Nie and S. Song, *Carbohydr. Polym.*, 2019, **203**, 110–118.
- 32 M. B. Wu, S. Huang, T. Y. Liu, J. Wu, S. Agarwal, A. Greiner and Z. K. Xu, *Adv. Funct. Mater.*, 2021, **31**, 2006806.
- 33 X. Wu, F. Yang, J. Gan, Z. Kong and Y. Wu, *Nanomaterials*, 2021, **11**, 1885.
- 34 C. Shao, M. Jiang, J. Zhang, Q. Zhang, L. Han and Y. Wu, *Appl. Surf. Sci.*, 2023, **609**, 155259.
- 35 T. Yang, Y. Li, H. Gui, D. Du, X. M. Song and F. Liang, *ACS Appl. Mater. Interfaces*, 2021, **13**, 25392–25399.
- 36 K. Wang, Y. Dong, Y. Yan, W. Zhang, C. Qi, C. Han, J. Li and S. Zhang, *Wood Sci. Technol.*, 2017, **51**, 395–411.
- 37 Y. Wang, Z. Tang, S. Lu, M. Zhang, K. Liu, H. Xiao, L. Chen, H. Wu and Y. Ni, *Holzforschung*, 2020, **74**, 799–809.
- 38 Y. Wang, W. Yan, M. Frey, M. V. D. Blanco, M. Schubert, M. Adobes-Vidal and E. Cabane, *Adv. Sustainable Syst.*, 2019, **3**, 1800070.
- 39 H. Meng, Y. Zhao, S. Wang, Y. Wang, Z. Xiao, H. Wang, D. Liang and Y. Xie, *Ind. Crops Prod.*, 2022, **183**, 114969.
- 40 X. Wu, F. Yang, J. Gan, W. Zhao and Y. Wu, *J. Mater. Res. Technol.*, 2021, **14**, 1820–1829.
- 41 Z. Wang, W. Zou, D. Sun, X. Ji and M. Yu, *Wood Sci. Technol.*, 2020, **54**, 1223–1239.
- 42 Y. Wu, X. Wu, F. Yang and J. Ye, *Polymers*, 2020, **12**, 668.
- 43 Y. Li, Z. Xiong, M. Zhang, Y. He, Y. Yang, Y. Liao, J. Hu, M. Wang and G. Wu, *Cellulose*, 2021, **28**, 11579–11593.
- 44 A. J. Wang, K. S. Liao, S. Maharjan, Z. Zhu, B. McElhenny, J. Bao and S. A. Curran, *Nanoscale*, 2019, **11**, 8565–8578.
- 45 Y. Hu, B. Zhao, S. Lin, X. Deng and L. Chen, *Int. J. Heat Mass Transfer*, 2020, **159**, 120063.
- 46 S. Janhom, *J. Environ. Chem. Eng.*, 2019, **7**, 103120.
- 47 L. Zhang, S. Lyu, Z. Chen and S. Wang, *Surf. Coat. Technol.*, 2018, **349**, 318–327.
- 48 J. Huang, S. Lyu, F. Fu, H. Chen and S. Wang, *RSC Adv.*, 2016, **6**, 106194–106200.
- 49 X. Chen, G. Du, A. Pizzi and X. Xi, *J. Wood Chem. Technol.*, 2020, **40**, 58–72.
- 50 J. Zhou, G. Gao, Y. Li, D. Wang, J. Hu, Y. Song and P. Chen, *Bioresources*, 2022, **17**, 384–399.
- 51 S. Wang, J. Shi, C. Liu, C. Xie and C. Wang, *Appl. Surf. Sci.*, 2011, **257**, 9362–9365.
- 52 Z. Zhu, S. Fu and L. A. Lucia, *ACS Sustainable Chem. Eng.*, 2019, **7**, 16428–16439.
- 53 L. Gao, Y. Lu, X. Zhan, J. Li and Q. Sun, *Surf. Coat. Technol.*, 2015, **262**, 33–39.
- 54 B. Yu, Y. Zhou, P. Li, W. Tu, P. Li, L. Tang, J. Ye and Z. Zou, *Nanoscale*, 2016, **8**, 11870–11874.
- 55 L. Gao, W. Gan, S. Xiao, X. Zhan and J. Li, *Ceram. Int.*, 2016, **42**, 2170–2179.
- 56 Q. Lu, R. Cheng, H. Jiang, S. Xia, K. Zhan, T. Yi, J. J. Morrell, L. Yang, H. Wan, G. Du and W. Gao, *Colloids Surf., A*, 2022, **647**, 129162.
- 57 M. Sun and K. Song, *Bioresources*, 2018, **13**, 1075–1087.
- 58 S. Wang, C. Wang, C. Liu, M. Zhang, H. Ma and J. Li, *Colloids Surf., A*, 2012, **403**, 29–34.
- 59 M. Liu, Y. Qing, Y. Wu, J. Liang and S. Luo, *Appl. Surf. Sci.*, 2015, **330**, 332–338.
- 60 H. Chang, K. Tu, X. Wang and J. Liu, *Bioresources*, 2015, **10**, 2585–2596.
- 61 Y. Wang, T. Tian and E. Cabane, *ACS Sustainable Chem. Eng.*, 2017, **5**, 11686–11694.



- 62 J. Wei, G. Zhang, J. Dong, H. Wang, Y. Guo, X. Zhou, C. Li, H. Liang, S. Gu, C. Li, X. Dong and Y. Li, *ACS Sustainable Chem. Eng.*, 2018, **6**, 11335–11344.
- 63 K. Maghsoudi, G. Momen, R. Jafari and M. Farzaneh, *Appl. Surf. Sci.*, 2018, **458**, 619–628.
- 64 X. Gao, L. Su, G. Q. Jiang, R. J. Pang and L. Lin, *Bioresources*, 2020, **15**, 3443–3457.
- 65 Y. Wang, S. Vitas, I. Burgert and E. Canbancane, *Wood Sci. Technol.*, 2019, **53**, 985–999.
- 66 Y. Ma, Z. Yin, C. Pei, X. Cui and Y. Zhou, *J. Porous Mater.*, 2016, **23**, 225–230.
- 67 G. Liu and T. Wang, *J. Funct. Biomater.*, 2016, **47**, 11186–11189.
- 68 T. Wang, X. Feng, J. Kong and C. Wong, *Adv. Eng. Mater.*, 2017, **19**, 1700147.
- 69 K. Nie, L. Xu, T. Qian, X. Shen and Q. Sun, *J. Wood Chem. Technol.*, 2020, **40**, 44–57.
- 70 Y. Yao, A. Gellerich, M. Zauner, X. Wang and K. Zhang, *Cellulose*, 2018, **25**, 1329–1338.
- 71 Q. Lu, H. Jiang, R. Cheng, S. Xia, K. Zhan, T. Yi, J. J. Morrelle, L. Yang, G. Du and W. Gao, *Ind. Crops Prod.*, 2021, **172**, 113952.
- 72 Z. Ding, W. Lin, W. Yang, H. Chen and X. Zhang, *Polymers*, 2022, **14**, 3062.
- 73 X. Han, Z. Wang, Q. Zhang and J. Pu, *Forests*, 2019, **10**, 750.
- 74 H. Chang, K. Tu, X. Wang and J. Liu, *RSC Adv.*, 2015, **5**, 30647–30653.
- 75 T. Arbatan, L. Zhang, X. Y. Fang and W. Shen, *Chem. Eng. J.*, 2012, **210**, 74–79.
- 76 D. Łukawski, A. Lekawa-Raus, F. Lisiecki, K. Koziol and A. Dudkowiak, *Prog. Org. Coat.*, 2018, **125**, 23–31.
- 77 J. Huang, S. Wang, S. Lyu and F. Fu, *Ind. Crops Prod.*, 2018, **122**, 438–447.
- 78 J. Wang, Y. Lu, Q. Chu, C. Ma, L. Cai, Z. Shen and H. Chen, *Polymers*, 2020, **12**, 813.
- 79 Y. Shen, Y. Wu, Z. Shen and H. Chen, *Coatings*, 2018, **8**, 144.
- 80 X. Deng, L. Mammen, H. J. Butt and D. Vollmer, *Science*, 2012, **335**, 67–70.
- 81 H. Liu, J. Huang, Z. Chen, G. Chen, K. Zhang, S. S. Al-Deyab and Y. Lai, *Chem. Eng. J.*, 2017, **330**, 26–35.
- 82 W. Zhang, D. Wang, Z. Sun, J. Song and X. Deng, *Chem. Soc. Rev.*, 2021, **50**, 4031–4061.
- 83 N. Wang, Q. Wang, S. Xu, L. Qu and Z. Shi, *Colloids Surf., A*, 2021, **608**, 125624.
- 84 A. Millionis, E. Loth and I. S. Bayer, *Adv. Colloid Interface Sci.*, 2016, **229**, 57–79.
- 85 B. Yuan, X. Ji, T. T. Nguyen, Z. Huang and M. Guo, *Appl. Surf. Sci.*, 2019, **467**, 1070–1075.
- 86 K. Chen, Xi. Zhou, D. Wang, J. Li and D. Qi, *Int. J. Biol. Macromol.*, 2022, **218**, 33–43.
- 87 T. Zhu, Y. Cheng, J. Huang, J. Xiong, M. Ge, J. Mao, Z. Liu, X. Dong, Z. Chen and Y. Lai, *Chem. Eng. J.*, 2020, **399**, 125746.
- 88 M. Cao, M. Tang, W. Lin, Z. Ding, S. Cai, H. Chen and X. Zhang, *Polymers*, 2022, **14**, 1953.
- 89 X. Wu, S. Zheng, D. A. Bellido-Aguilar, V. V. Silberschmidt and Z. Chen, *Mater. Des.*, 2018, **140**, 516–523.
- 90 W. Zhao, L. Xiao, X. He, Z. Cui, J. Fang, C. Zhang, X. Li, G. Li, L. Zhang and Y. Zhang, *Opt. Laser Technol.*, 2021, **141**, 107115.
- 91 R. Gao, Y. Huang, W. Gan, S. Xiao, Y. Gao, B. Fang, X. Zhang, B. Lyu, R. Huang and J. Li, *Chem. Eng. J.*, 2022, **442**, 136338.
- 92 Z. Chen, X. Su, W. Wu, J. Zhou, T. Wu, Y. Wu, H. Xie and K. Li, *Carbon*, 2023, **201**, 577–586.
- 93 P. L. Wang, C. Ma, Q. Yuan, T. Mai and M. G. Ma, *J. Colloid Interface Sci.*, 2022, **606**, 971–982.
- 94 M. Liu, Z. Wang, P. Liu, Z. Wang, H. Yao and X. Yao, *Sci. Adv.*, 2019, **5**, eaaw5643.
- 95 T. Wang, H. Feng, W. Wang, L. Cao, C. Ma, X. Qin, J. Piao and S. Chen, *Composites, Part B*, 2022, **240**, 110002.
- 96 C. Li, P. Wang, D. Zhang and S. Wang, *ACS Appl. Mater. Interfaces*, 2022, **14**, 45988–46000.
- 97 Y. Lu, S. Sathasivam, J. Song, C. R. Crick, C. J. Carmalt and I. P. Parkin, *Science*, 2015, **347**, 1132–1135.
- 98 J. Sun, H. Guo, J. Ribera, C. Wu, K. Tu, M. Binelli, G. Panzarasa, F. W. M. R. Schwarze, Z. L. Wang and I. Burgert, *ACS Nano*, 2020, **14**, 14665–14674.
- 99 F. Ram, J. Garemark, Y. Li and L. Berglund, *Composites, Part A*, 2022, **160**, 107057.
- 100 X. Li, C. Jiang, F. Zhao, Y. Shao, Y. Ying and J. Ping, *Nano Energy*, 2020, **73**, 104738.
- 101 A. Elzaabalawy and S. A. Meguid, *Chem. Eng. J.*, 2020, **398**, 125403.
- 102 X. Jiao, M. Li, X. Yu, W. S. Y. Wong and Y. Zhang, *Chem. Eng. J.*, 2021, **420**, 127606.
- 103 F. Wang, J. Y. Li, J. Pi, F. Song, Y. Q. Luo, X. L. Wang and Y. Z. Wang, *Chem. Eng. J.*, 2021, **421**, 127793.
- 104 G. Liu, H. Xia, W. Zhang, L. Lang, H. Geng, L. Song and Y. Niu, *ACS Appl. Mater. Interfaces*, 2021, **13**, 12509–12520.
- 105 M. Liu, Y. Hou, J. Li, L. Tie and Z. Guo, *Colloids Surf., A*, 2018, **553**, 645–651.
- 106 H. Zhang, X. Ji, L. Liu, J. Ren, F. Tao and C. Qiao, *Chem. Eng. J.*, 2020, **402**, 126160.
- 107 X. Zhou, J. Liu, W. Liu, W. Steffen and H. J. Butt, *Adv. Mater.*, 2022, **34**, 2107901.
- 108 D. Zhang, G. Wu, H. Li, Y. Cui and Y. Zhang, *Chem. Eng. J.*, 2021, **406**, 126753.
- 109 C. Huang, F. Wang, D. Wang and Z. Guo, *New J. Chem.*, 2020, **44**, 1194–1203.
- 110 M. Long, S. Peng, X. Y. ang, W. Deng, N. Wen, K. Miao, G. Chen, X. Miao and W. Deng, *ACS Appl. Mater. Interfaces*, 2017, **9**, 15857–15867.
- 111 X. Jiao, M. Li, X. Yu, S. Yang and Y. Zhang, *Chem. Eng. J.*, 2022, **446**, 137336.
- 112 L. Zhang, C. H. Xue, M. Cao, M. M. Zhang, M. Li and J. Z. Ma, *Chem. Eng. J.*, 2017, **320**, 244–252.
- 113 H. Xie, J. Wei, S. Duan, Q. Zhu, Y. Yang, K. Chen, J. Zhang, L. Li and J. Zhang, *Chem. Eng. J.*, 2022, **428**, 132585.
- 114 Y. Qing, C. Long, K. An, C. Hu and C. Liu, *J. Colloid Interface Sci.*, 2019, **548**, 224–232.
- 115 M. Yu, Z. Cui, F. Ge, L. Lei and X. Wang, *Composites, Part B*, 2019, **179**, 107431.



- 116 S. K. Lahiri, P. Zhang, C. Zhang and L. Liu, *ACS Appl. Mater. Interfaces*, 2019, **11**, 10262–10275.
- 117 G. Ren, Y. Song, X. Li, B. Wang, Y. Zhou, Y. Wang, B. Ge and X. Zhu, *J. Colloid Interface Sci.*, 2018, **522**, 57–62.
- 118 T. Zhu, S. Li, J. Huang, M. Mihailiasa and Y. Lai, *Mater. Des.*, 2017, **134**, 342–351.
- 119 L. Wang, Y. Chen, L. Lin, H. Wang, X. Huang, H. Xue and J. Gao, *Chem. Eng. J.*, 2019, **362**, 89–98.
- 120 J. Luo, S. Gao, H. Luo, L. Wang, X. Huang, Z. Guo, X. Lai, L. Lin, R. K. Y. Li and J. Gao, *Chem. Eng. J.*, 2021, **406**, 126898.
- 121 S. Li, K. Page, S. Sathasivam, F. Heale, G. He, Y. Lu, Y. Lai, G. Chen, C. J. Carmalt and I. P. Parki, *J. Mater. Chem. A*, 2018, **6**, 17633–17641.
- 122 X. J. Guo, C. H. Xue, S. Sathasivam, K. Page, G. He, J. Guo, P. Promdet, F. L. Heale, C. J. Carmalt and I. P. Parkin, *J. Mater. Chem. A*, 2019, **7**, 17604–17612.
- 123 S. Barthwal and S. H. Lim, *J. Membr. Sci.*, 2021, **618**, 118716.
- 124 T. Ma, L. Li, C. Mei, Q. Wang and C. Guo, *J. Mater. Sci.*, 2021, **56**, 5624–5636.
- 125 X. F. Zhang, J. P. Zhao and J. M. Hu, *Adv. Mater. Interfaces*, 2017, **4**, 1700177.
- 126 Y. Li, H. Li, J. Wu, X. Yang, X. Jia, J. Yang, D. Shao, L. Feng, S. Wang and H. Song, *Appl. Surf. Sci.*, 2022, **600**, 154177.
- 127 Y. Jin, T. Zhang, J. Zhao, Y. Zhao, C. Liu, J. Song, X. Hao, J. Wang, K. Jiang, S. Fan and Q. Li, *Carbon*, 2021, **178**, 616–624.
- 128 K. Tu, X. Wang, L. Kong and H. Guan, *Mater. Des.*, 2018, **140**, 30–36.
- 129 J. Wei, B. Li, N. Tian, J. Zhang, W. Liang and J. Zhang, *Adv. Funct. Mater.*, 2022, **32**, 2206014.
- 130 Y. Liao, S. Deng, Y. Qing, H. Xu, C. Tian and Y. Wu, *J. Energy Chem.*, 2023, **76**, 566–575.
- 131 Q. Zhou, K. Lee, K. Kim, J. Park, J. Pan, J. Bae, J. Baik and T. Kim, *Nano Energy*, 2019, **57**, 903–910.

